Complementary roles for parvalbumin and somatostatin interneurons in the generation of hippocampal gamma oscillations

Pantelis Antonoudiou[1], Yu Lin Tan[1], Georgina Kontou[3], A. Louise Upton[1,2] and Edward O. Mann[1,2]

[1]Department of Physiology, Anatomy and Genetics, University of Oxford, Oxford, OX1 3PT, UK

[2]Oxford Ion Channel Initiative, University of Oxford, OX1 3PT, Oxford, UK

[3]Neuroscience, Physiology and Pharmacology, University College London

Abstract

Gamma-frequency oscillations (30-120 Hz) can be separated into fast (>60 Hz) and slow oscillations, with different roles in neuronal encoding and information transfer. While synaptic inhibition is important for synchronization across the gamma-frequency range, the role of distinct interneuronal subtypes in fast and slow gamma states remains unclear. Here, we used optogenetics to examine the involvement of parvalbumin (PV+) and somatostatin (SST+) expressing interneurons in gamma oscillations in the mouse hippocampal CA3 *ex vivo*. Disrupting either PV+ or STT+ interneuron activity, via either photo-inhibition or photo-excitation, led to a decrease in the power of cholinergically-induced slow gamma oscillations. Furthermore, photo-excitation of SST+ interneurons induced fast gamma oscillations, which depended on both synaptic excitation and inhibition. Our findings support a critical role for both PV+ and SST+ interneurons in slow hippocampal gamma oscillations, and further suggest that STT+ interneurons are capable of switching the network between slow and fast gamma states.

Introduction

Gamma oscillations (30 - 120 Hz) are a common feature of active cortical networks, which have been proposed to contribute to local gain control (Sohal *et al.*, 2009; Cardin *et al.*, 2009; Sohal, 2016) and facilitate transmission between synchronised neuronal assemblies (Fries, 2005; Akam & Kullmann, 2010; Fries, 2015). While the function of gamma oscillations remains debated (Burns, Xing & Shapley, 2011; Butler & Paulsen, 2014; Bastos, Vezoli & Fries, 2015; Ray & Maunsell, 2015; Womelsdorf & Everling, 2015; Lasztóczi & Klausberger, 2016; Sohal, 2016), changes in these rhythms continue to act as a useful marker of function and dysfunction in cortical circuit operations (Bragin *et al.*, 1995; Fries *et al.*, 2001; Herrmann & Demiralp, 2005; Uhlhaas & Singer, 2006; Basar-Eroglu *et al.*, 2007; Uhlhaas & Singer, 2010; Yamamoto *et al.*, 2014; Spellman *et al.*, 2015). There is a general consensus that the generation of gamma rhythms depends upon the spiking of inhibitory interneurons, which synchronise the firing of excitatory pyramidal cells via fast synaptic inhibition (Whittington, Traub & Jefferys, 1995; Penttonen *et al.*, 1998a; Csicsvari *et al.*, 2003; Hajos, 2004; Mann *et al.*, 2005; Hasenstaub *et al.*, 2005; Bartos, Vida & Jonas, 2007; Buzsáki & Wang, 2012; Kim *et al.*, 2016; Chen *et al.*, 2017; Veit *et al.*, 2017). Specifically, parvalbumin-expressing (PV+) interneurons, which target the perisomatic domain of pyramidal neurons, are thought to play the key role in generating and maintaining gamma oscillations in the brain (Csicsvari *et al.*, 2003; Hajos, 2004; Mann *et al.*, 2005; Gloveli *et al.*, 2005; Hájos & Paulsen, 2009; Tukker *et al.*, 2013; Cardin, 2016; Penttonen *et al.*, 1998b). PV+ interneurons are adapted for fast synchronisation of network activity, as they resonate at gamma frequencies and exert strong perisomatic inhibition that is capable of precisely controlling spike timing (Pike *et al.*, 2000; Pouille & Scanziani, 2001; Cardin *et al.*, 2009; Bartos & Elgueta, 2012; Hu, Gan & Jonas, 2014; Kohus *et al.*, 2016). Moreover, at least in the CA3 hippocampal subfield, the gamma oscillations recorded in the local field potential appear

to directly reflect rhythmic perisomatic inhibitory currents (Mann *et al.*, 2005; Oren, Hájos & Paulsen, 2010).

Recently, a selective role for PV+ interneurons in gamma-frequency synchronisation has been challenged by several studies performed in the primary visual cortex (Chen *et al.*, 2017; Veit *et al.*, 2017; Hakim, Shamardani & Adesnik, 2018). In this brain region, it was shown that dendrite-targeting somatostatin-expressing (SST+) interneurons were the main contributors for the generation of slow gamma oscillations, while PV+ interneurons were more important for higher frequency synchronisation (Chen *et al.*, 2017). Previous studies have found analogous roles for SST+ and PV+ interneurons in low- and high-frequency network synchronisation (Beierlein, Gibson & Connors, 2000; Gloveli *et al.*, 2005; Tukker *et al.*, 2007; Craig & McBain, 2015). However, it is not yet clear if it is the frequency tuning of each interneuronal circuit that varies across brain areas, or whether SST+ interneurons might play a more generic role in the generation of slow gamma oscillations.

The hippocampus displays both slow and fast gamma rhythms during theta activity, with slow gamma generated in CA3 and fast gamma propagated from entorhinal cortex (Bragin *et al.*, 1995; Colgin *et al.*, 2009; Schomburg *et al.*, 2014; Lasztóczi & Klausberger, 2016). The circuitry for slow gamma oscillations is preserved in hippocampal slices (Fisahn *et al.*, 1998), and these models have been used extensively to show that PV+ interneurons are strongly phase-coupled to gamma oscillations, and contribute to rhythmogenesis (Hajos, 2004; Mann *et al.*, 2005; Gloveli *et al.*, 2005; Gulyás *et al.*, 2010). However, the majority of interneurons are phase-coupled to ongoing slow gamma oscillations (Hajos, 2004; Gloveli *et al.*, 2005; Oren *et al.*, 2006), and it may be that SST+ interneurons play an important role in synchronising PV+ networks. Indeed, whether specific classes of CA3 interneuron are necessary and sufficient for the generation of slow gamma oscillations has not yet been tested. Here, we took advantage of optogenetic techniques (Nagel *et al.*, 2003; Chow

74 *et al.*, 2010; Boyden *et al.*, 2005) to test the involvement of PV+ and SST+ interneurons in
75 cholinergically-induced gamma oscillations in the CA3 of acute hippocampal slices.

76

77 # Results

78 ## PV+ interneuron activity is necessary for cholinergically-induced gamma oscillations
79 ## in hippocampal CA3

80 In order to test if the activity of PV+ interneurons is necessary for the generation of slow
81 hippocampal gamma oscillations, we took advantage of optogenetic photo-inhibition (Chow *et al.*,
82 2010). We injected PV-cre mice with AAV carrying the inhibitory proton pump archaerhodopsin
83 (Arch3-eYFP or ArchT-GFP). Expression of Arch in PV-cre mice was restricted to the pyramidal cell
84 layer indicating selective expression in perisomatic targeting PV+ interneurons (Fig. 1a) (Somogyi &
85 Klausberger, 2005; Royer *et al.*, 2012; Hu, Gan & Jonas, 2014). Intracellular recordings performed in
86 opsin expressing cells demonstrated that these cells were fast-spiking and that sustained light
87 illumination was able to produce robust hyperpolarisation, indicating functional expression of Arch
88 in PV+ interneurons (Supplementary Fig. 1d-e).

89 Gamma oscillations were induced in hippocampal slices from PV-Arch mice in area CA3 using bath
90 application of the cholinergic agonist carbachol (Cch - 5 µM). Local field potential recordings from
91 the CA3 pyramidal cell layer revealed robust gamma oscillations that were centred around 30 – 40
92 Hz with clear side peaks in the autocorrelogram (Supplementary Fig. 1a-c), as has been reported
93 previously (Fisahn *et al.*, 1998; Hajos, 2004; Mann *et al.*, 2005). Overall, sustained photo-inhibition
94 of PV+ interneurons using LED illumination (< 5mW) significantly decreased gamma power area
95 (0.82 +/- 0.068 of baseline period, $t = 2.59$, $p = 0.029$, one sample t-test; Fig. 1 b-d), although
96 increases in power were observed in some slices (Fig. 1d). A significant suppression was also

observed in the period of 0.5 - 1.5 seconds following light illumination termination (0.85 +/- 0.022 of baseline period, $t = 6.70$, $p < 0.001$, one sample t-test; Fig. 1d). However, the light-induced changes in gamma power were reversible, as there were no significant changes in the gamma power area recorded during the baseline periods across trials ($F(4, 116) = 0.68$, $p = 0.61$, rmANOVA). The changes in gamma power were not accompanied by a consistent change in gamma frequency ($F(1.44, 43.23) = 1.25$, $p = 0.288$, rmANOVA; Fig. 1e), although there was a significant correlation between the changes in frequency and power area ($t = 2.77$, $p = 0.01$, Pearson correlation, Fig. 1f), suggesting a consistent disturbance to endogenous oscillatory activity.

While LED photo-inhibition of PV+ interneurons significantly modulated gamma power, the oscillations did not collapse. Pyramidal neurons make strong recurrent connections with PV+ interneurons (Mann, Radcliffe & Paulsen, 2005; Oren *et al.*, 2006; Hofer *et al.*, 2011; Packer & Yuste, 2011; Bartos & Elgueta, 2012; Kohus *et al.*, 2016), and it might be hard to break these feedback loops with photo-induced inhibitory currents. To test this possibility, we used long-lasting laser illumination with the prospect of biochemically silencing PV+ interneurons, by preventing synaptic release via terminal alkalisation (El-Gaby *et al.*, 2016). PV+ interneurons expressing ArchT-GFP were illuminated with sustained green laser light (532 nm, approx. 18 mW for 20 seconds). Similar to the LED experiments, there were inconsistent network responses to PV+ interneuron photo-inhibition at the beginning of laser illumination (1.00 +/- 0.087 of baseline period, $t = 0.04$, $p = 1.00$, one sample t-test; Fig. 1g&h). However, the power of the oscillation consistently decreased during sustained laser illumination (0.57 +/- 0.086 of baseline period, $t = 5.00$, $p < 0.001$, one sample t-test; Fig. 1g&h) and remained suppressed in the light-off period following laser stimulation (0.78 +/- 0.071 of baseline period, $t = 3.17$, $p = 0.022$, one sample t-test; Fig. 1g, h). There was no consistent effect on the frequency of the oscillations ($F(1.92, 23.08) = 7.77$, $p = 0.003$, rmANOVA; Fig. 1g&i). Laser illumination of PV+ interneurons expressing only control fluorophore did not alter gamma oscillation power nor frequency (Supplementary Fig. 1g-i). This slow and selective process of decreasing

122 gamma power is consistent with biochemical silencing of synaptic terminals (El-Gaby *et al.*, 2016).
123 These results further support the importance of PV+ interneuron activity in generating gamma
124 oscillations in hippocampal area CA3 (Hajos, 2004; Mann *et al.*, 2005; Gulyás *et al.*, 2010; Tukker *et*
125 *al.*, 2013). Residual gamma oscillations following photo-inhibition of PV+ interneurons may reflect
126 incomplete transfection of the PV+ network or the presence of a distinct oscillatory circuit.

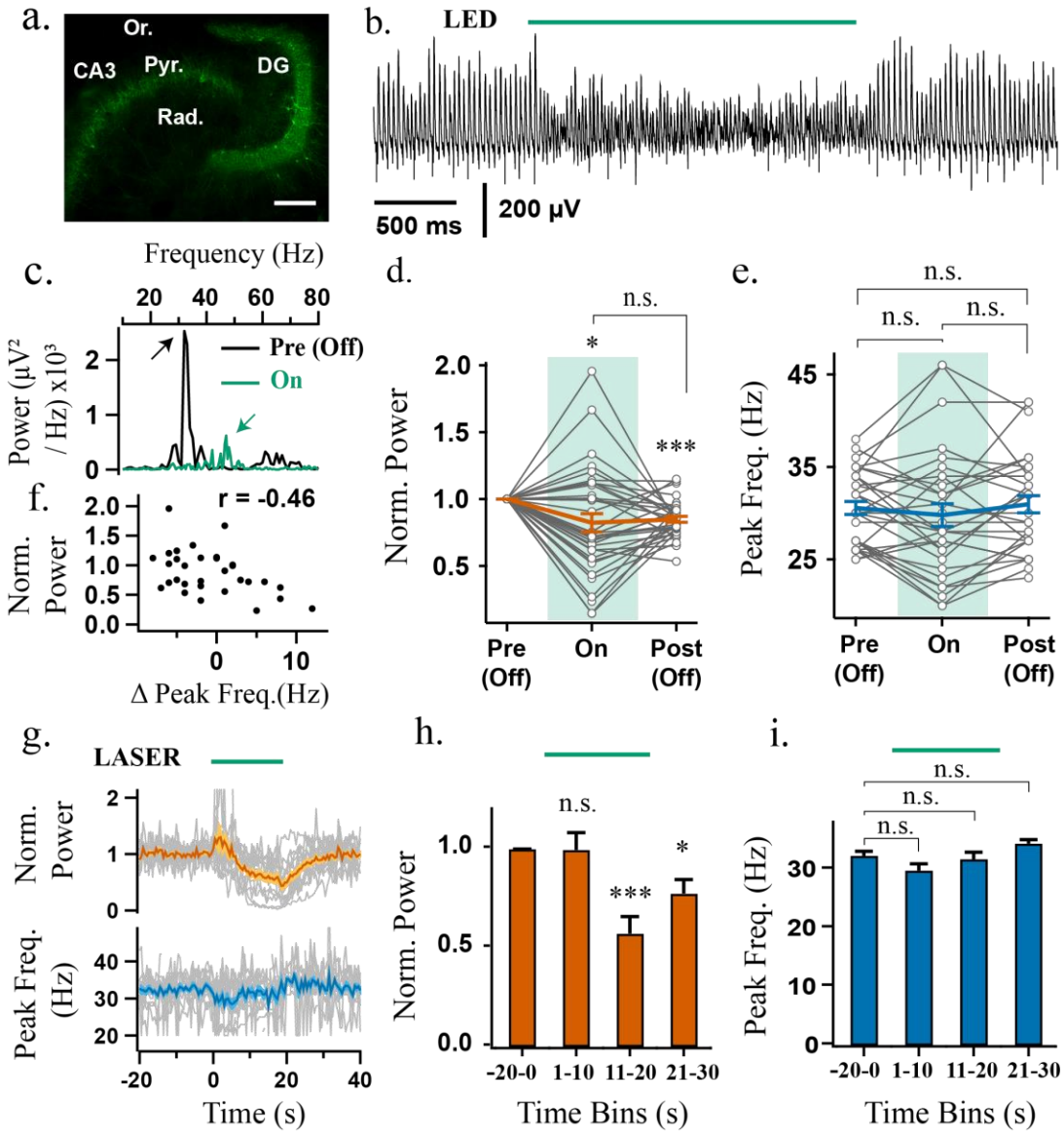

Figure 1: Sustained photo-inhibition of PV+ interneurons suppresses the power of gamma oscillations. a-e) photo-inhibition with LED and g-i) photo-inhibition with laser experiments. a) Confocal image of ventral hippocampus slice from a PV-cre mouse injected intrahippocampally with AAV-Arch3 eYFP. CA3 = Cornu Ammonis 3, DG = Dentate Gyrus, Pyr. = stratum Pyramidale, Rad. = stratum Radiatum, Or. = Stratum Oriens. Scale bar = 200 µm. b) LFP recording from CA3 stratum pyramidale illustrating effect of PV+ interneuron photo-inhibition (LED, 530 nm, approx. 4.25 mW) on gamma oscillations induced by the application of 5 µM Cch. c) Representative power spectra before (black) and during (green) LED illumination (arrows indicate power spectrum peaks). d) Power area in the 20 -100 Hz band normalised to baseline (Pre (Off)) during (On) and after LED stimulation (Off (Post)) (n = 35). e) Peak frequency for experiments when the oscillation was not abolished (n = 31/35). f) Power area change versus peak frequency difference recorded between stimulation and baseline periods. g) Stronger photoinhibition was achieved using high power laser illumination (approx. 18.6 mW). Top: Change in power area normalised to baseline. Bottom: Peak frequency of the oscillation calculated in 1 second bins across experiments (n = 14). h) Mean change in power area normalised to baseline (n = 14). i) Mean peak frequency for trials when the oscillation was not abolished (n = 13). *p < 0.05, **p < 0.01, ***p < 0.001, n.s. p >= 0.05. Changes in peak frequency were analysed using rmANOVA, followed by post-hoc paired t-tests with correction for multiple comparisons. Solid brackets represent paired t-tests and standalone star symbols represent one-sample t-test versus normalised baseline. Grey lines represent single experiments. Error bars and shaded area are SEM and coloured line the population mean.

128

Supplementary Figure 1 (Supporting Figure 1)

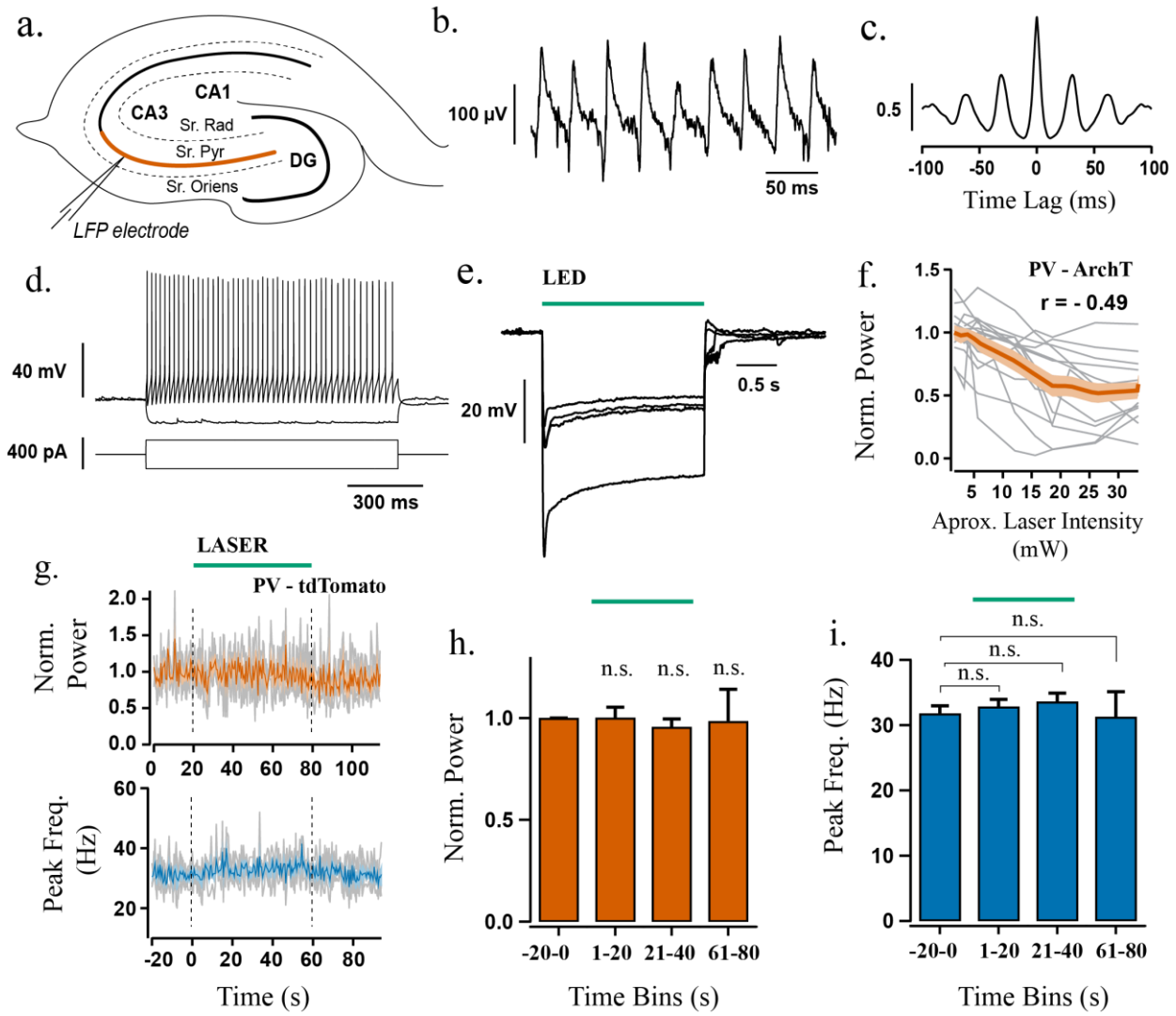

Supplementary Figure 1: a-c) Recording gamma oscillations in hippocampal CA3. a) Illustration of the electrophysiological setup used to record gamma oscillations using a glass field electrode in stratum pyramidale of hippocampal area CA3 (coloured line indicates the CA3 area where recordings were obtained). b) Representative LFP recording from the ventral CA3 area obtained by the application of 5 µM Cch. c) Autocorrelogram of the recording in b) illustrating that the oscillation is rhythmic with a period of 31 ms. d-e) Validation of functional Arch expression in PV+ neurons. d) Current clamp recording of an ArchT-GFP expressing PV+ cell from CA3 area in response to steps of depolarising and hyperpolarising current injections. e) Potent hyperpolarisation of four PV+ interneurons during green light illumination in aCSF (1.45 mW). f) Power change between the last half of laser stimulation from baseline against approximate light intensity. Grey lines represent single experiments (n = 14). The orange line is the average response and the orange shaded area represents SEM. g-i) Responses to laser illumination in control slices from PV-Ai9 mice. g) Top: Change in power-area normalised to baseline calculated in 1 second bins across experiments (n = 4). Bottom: Peak frequency of the oscillation calculated in 1 second bins across experiments (n = 4). Time between dotted lines indicates the duration of laser illumination (duration of approx. 1 minute and a light intensity of approx. 25-41 mW). h-i) quantification of normalised power and peak frequency. n.s. p >= 0.05. Changes in peak frequency were analysed using rmANOVA, followed by post-hoc paired t-tests with correction for multiple comparisons. Solid brackets represent paired t-tests and standalone star symbols represent one-sample t-test versus normalised baseline. Error bars and shaded area are SEM and coloured line the population mean.

SST+ interneurons are necessary for Cch-induced gamma oscillations in hippocampal area ca3

To examine if SST+ interneuron activity is also required during Cch-induced gamma oscillations in CA3, we injected the AAV-Arch vector (Arch3-eYFP or ArchT-GFP) intrahippocampally in SST-cre mice. Expression of Arch was restricted to the strata oriens, radiatum and lacunosum moleculare (Fig. 2a), suggesting expression in SST+ dendrite-targeting interneurons (Ma *et al.*, 2006; Lovett-Barron *et al.*, 2012; Muller & Remy, 2014; Urban-Ciecko & Barth, 2016). Whole-cell recordings were performed in opsin positive cells and indicated functional expression of Arch (n = 4, Supplementary Fig. 2a-b).

Unlike the experiments with PV+ photo-inhibition, sustained photo-inhibition of SST+ interneurons using LED illumination (< 5mW) reliably decreased gamma oscillation power (0.69 +/- 0.057 of baseline period, $t = 5.40$, $p < 0.001$, one sample t-test; Fig. 2c, d), which remained suppressed in the immediate period following SST+ interneuron photoinhibition (0.76 +/- 0.039 of baseline period, $t = -6.26745$, $p < 0.001$, one sample t-test; Fig. 1d). This post-light suppression was reversed from trial to trial ($F(4, 164) = 2046$, $p = 0.048$, rmANOVA; all paired t-tests $t > 2.81$, $p > 0.07$). In addition, light stimulation significantly modulated oscillation frequency ($F(1.25, 39.97) = 22.60$, $p < 0.001$, rmANOVA), with an increase in frequency from 37.79 +/- 1.083 Hz to 43.00 +/- 1.466 Hz during light stimulation ($t = 4.74$, $p < 0.01$, paired t-test), which reversed following light offset (Fig. 2e).

Stronger laser illumination in the first half of the stimulation period (532 nm, approx. 18 mW for 20 s) had similar effects as the LED experiment. Specifically, the power of Cch gamma oscillations decreased (0.70 +/- 0.064 of baseline, $t = 4.76$, $p < 0.01$, one-sample t-test), and the peak frequency increased (34.22 +/- 1.191 Hz to 38.60 +/- 1.868 Hz, $t = 3.93$, $p = 0.017$, paired t-test; rmANOVA, $F(1.36, 13.63) = 5.47$, $p = 0.027$; Fig. 2g-i). During the second half of the stimulation period, gamma power was strongly suppressed (0.35 +/-0.090 of baseline, $t = 7.23$, $p < 0.01$, one sample t-test; Fig.

153 2g-h), often resulting in oscillation collapse (7/13 slices). This could indicate that silencing SST+
154 interneurons is sufficient to disrupt the hippocampal network during gamma oscillations and that
155 SST+ interneuron activity is necessary for proper maintenance of Cch-induced oscillations in the CA3
156 area of the hippocampus. Moreover, the frequency of the Cch-gamma oscillations remains
157 upregulated for the whole duration of laser illumination when the oscillations do not collapse (Fig.
158 2i vs Supplementary Fig.2d), but in each case remained below 60 Hz, suggesting that SST+
159 interneurons can exert strong control over the frequency of slow gamma oscillations.

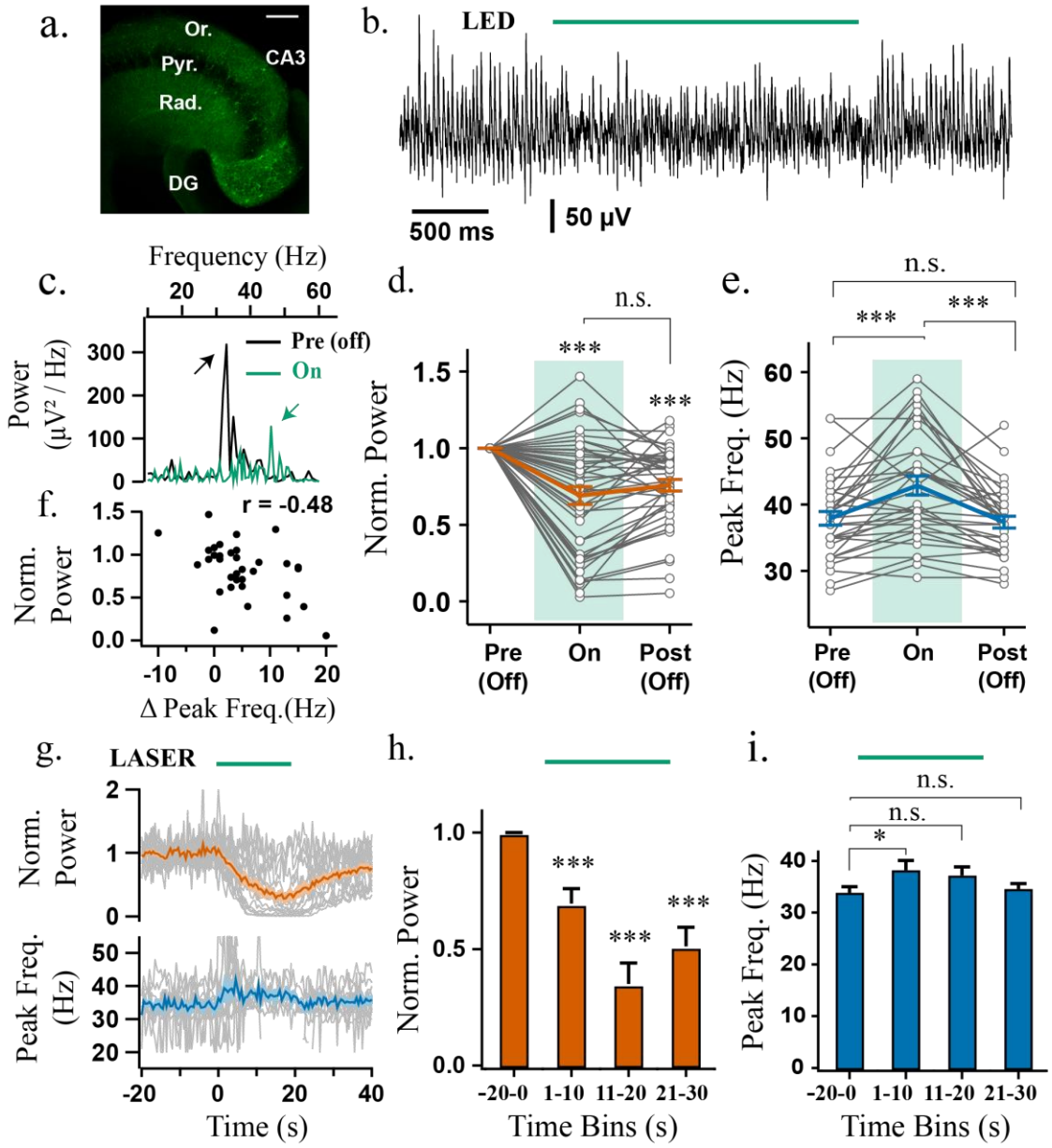

Figure 2: Sustained photo-inhibition of SST+ interneurons suppresses gamma power and increases frequency. a) Confocal image of ventral hippocampus slice from SST-cre mice with eYFP-Arch3 expression. CA3 = Cornu Ammonis 3, DG = Dentate Gyrus, Pyr. = stratum Pyramidale, Rad. = stratum Radiatum, Or. = Stratum Oriens. Scale bar = 200 µm. b) Representative LFP recordings from CA3 area illustrating effect of SST+ interneuron photo-inhibition (LED, 530 nm, approx. 4.25 mW) on gamma oscillations along with c) its respective power spectrum (arrows indicate power spectrum peaks). d) Power area in the 20 -100 Hz band normalised to baseline (Pre (Off)) during (On) and after LED stimulation (Post (Off)) (n = 44). e) Peak frequency for experiments when the oscillation was not abolished (n = 33/44). f) Power area change against peak frequency difference between stimulation and baseline periods. g) Top: Change in power-area normalised to baseline and Bottom: Peak frequency of the oscillation calculated in 1 second bins across experiments with high-power laser stimulation (approx. 18.6 mW; n = 17). h) Average power change normalised to baseline (n = 17). i) Average peak frequency (n = 11/17). *p < 0.05, **p < 0.01, ***p < 0.001, n.s. p >= 0.05. Changes in peak frequency were analysed using rmANOVA, followed by post-hoc paired t-tests with correction for multiple comparisons. Solid brackets represent paired t-tests and standalone star symbols represent one-sample t-test versus normalised baseline. Grey lines represent single experiments, error bars and shaded area are SEM and coloured line the population average.

161

Supplementary Figure 2 (Supporting Figure 2)

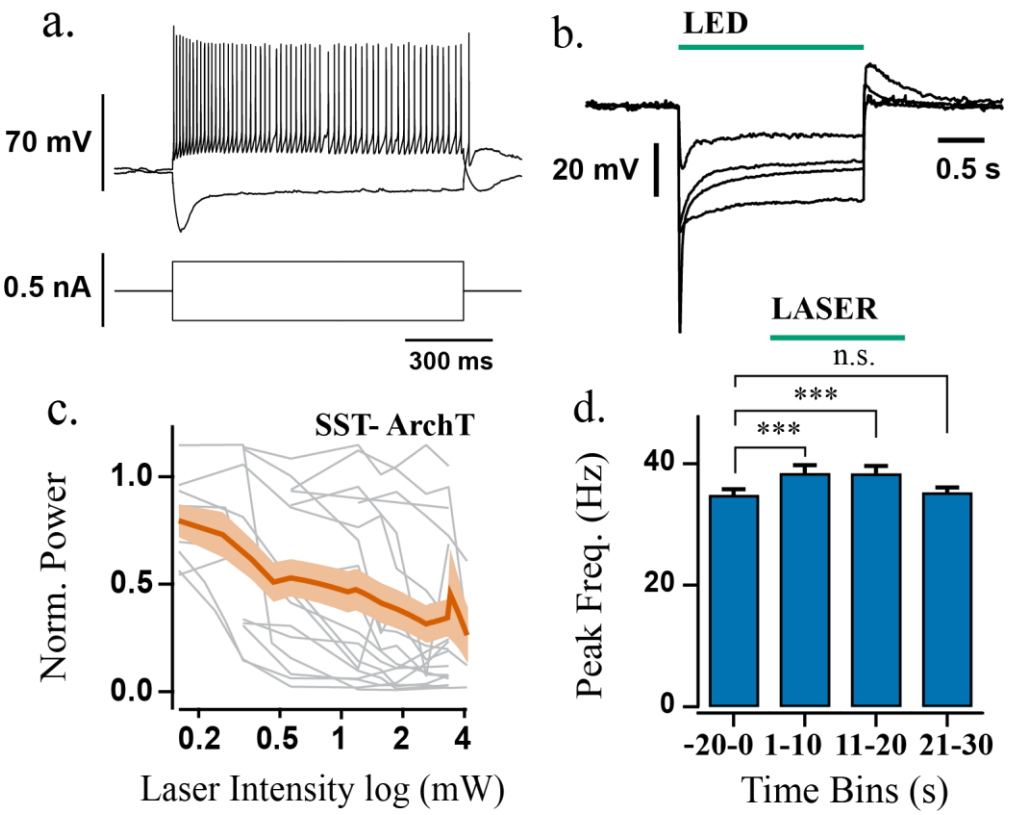

Supplementary Figure 2: a-b) Validation of functional opsin expression in SST+ interneurons. a) Current clamp recording of an SST+ cell from CA3 area in response to steps of depolarising and hyperpolarising current injections. b) Potent hyperpolarisation of four SST+ interneurons during green light illumination (1.45 mW). c-d) Effects of laser power on network activity. c) Power change between the last half of laser stimulation to baseline against approximate light intensity (n = 17). Coloured line represents the average and shaded area the SEM. d) Average peak frequency for half-maximal response of SST+ interneuron photo-inhibition (light intensity for each experiment that changed power-area by half of the maximum response). rmANOVA, $F(3, 48) = 19.27$, $p < 0.001$; ***$p < 0.001$, rmANOVA followed by post-hoc paired t-test for multiple comparisons. Solid brackets represent paired t-tests.

162

163

Rhythmic synchronisation of the hippocampal network by perisomatic and dendritic inhibition

The experiments using photo-inhibition indicate that the generation of gamma oscillations in hippocampal area CA3 involves the endogenous recruitment of both PV+ and SST+ interneurons. In order to test whether the activation of PV+ or SST+ interneurons is sufficient to synchronise the hippocampal network at gamma frequencies, we next examined cell type-specific photo-stimulation using Channelrhodopsin 2 (ChR2) (Nagel *et al.*, 2003; Boyden *et al.*, 2005). Injection of AAV-ChR2-mCherry produced similar expression patterns as Arch in both PV- and SST-Cre mouse lines (Fig. 3a, b). Photo-stimulation of ChR2-expressing PV+ interneurons at 40 Hz (1 ms pulse width) entrained ongoing oscillations in 14/18 experiments (>2mW; n = 12 at 5.5 mW, n = 6 at 2.2 mW - merged due to similar effects; Fig. 3c, f and Supplementary Fig. 3ai). In the remaining 4 out of 18 experiments the ongoing oscillations were not entrained (Fig. 3f; Supplementary Fig. 3aiii). This effect was likely observed due to low ChR2 expression, as pulses with longer width (5 ms) entrained the oscillation in the same experiments (Supplementary Fig. 3b-c). Thus, PV+ interneurons are sufficient to synchronise the hippocampal network at gamma frequencies.

Rhythmic photo-stimulation of SST+ interneurons reliably entrained ongoing oscillations in 19 out of 22 experiments (>2mW; n = 13 at 5.5 mW, n = 9 at 2.2 mW - merged due to similar effects; Fig. 3d, g). In the remaining 3 out of 22 oscillations were abolished during 40 Hz photo-stimulation. These results indicate that transient activation of SST+ dendrite-targeting interneurons is also sufficient to synchronise the hippocampal network at gamma frequencies. Activation of PV+ and SST+ interneurons produced opposite deflections in the pulse-locked waveform of the LFP recorded in the stratum pyramidale (Fig. 3c-e), as might be expected from the somatodendritic profile of their axon terminations. However, activation of SST+ interneurons was sometimes accompanied by an initial fast negative component (Fig. 3e), which was reminiscent of a population spike arising from

188 the synchronised firing of excitatory cells in the hippocampus (Andersen, Bliss & Skrede, 1971;
189 Wierenga & Wadman, 2003), despite the sparsity of SST+ axons in this layer.

190 To study the SST+ induced waveform in isolation, we repeated the same experiment in quiescent
191 slices, perfused only with aCSF. Blue light pulses (1 ms width) at 40 Hz induced strong pulse-locked
192 field responses with fast-negative deflections, which were resistant to glutamate receptor blockers
193 (Supplementary Fig. 3d-f), but were followed by a glutamate receptor-mediated positive deflection.
194 The fast-negative deflections did not appear to reflect fast GABAergic transmission, as application
195 of $GABA_A$ receptor ($GABA_AR$) blockers lead to light-induced epileptiform bursts (n = 4;
196 Supplementary Fig. 3g). These results suggest that SST+ interneuron photo-activation generates
197 network excitation, that is not mediated through $GABA_ARs$, at the onset of light illumination. We did
198 not observe ChR2 expression in CA3 pyramidal neurons during intracellular recordings (n = 18,
199 supplementary Fig. 5e), although there have been reports of off-target expression in SST+
200 interneurons of juvenile animals (Taniguchi *et al.*, 2011). An alternative possibility is that robust
201 activation of a dense plexus of SST+ axons in the dendritic layers is sufficient to induce spiking in
202 pyramidal neurons via ephaptic coupling (Ferenczi *et al.*, 2016a). Either scenario makes it difficult to
203 interpret the results of pulsed stimulation in the SST-ChR2 mice, but any electrically-mediated
204 bystander effects are likely to occur during stimulus onset (maximal hypersynchrony), and may be
205 less relevant during more sustained patterns of stimulation.

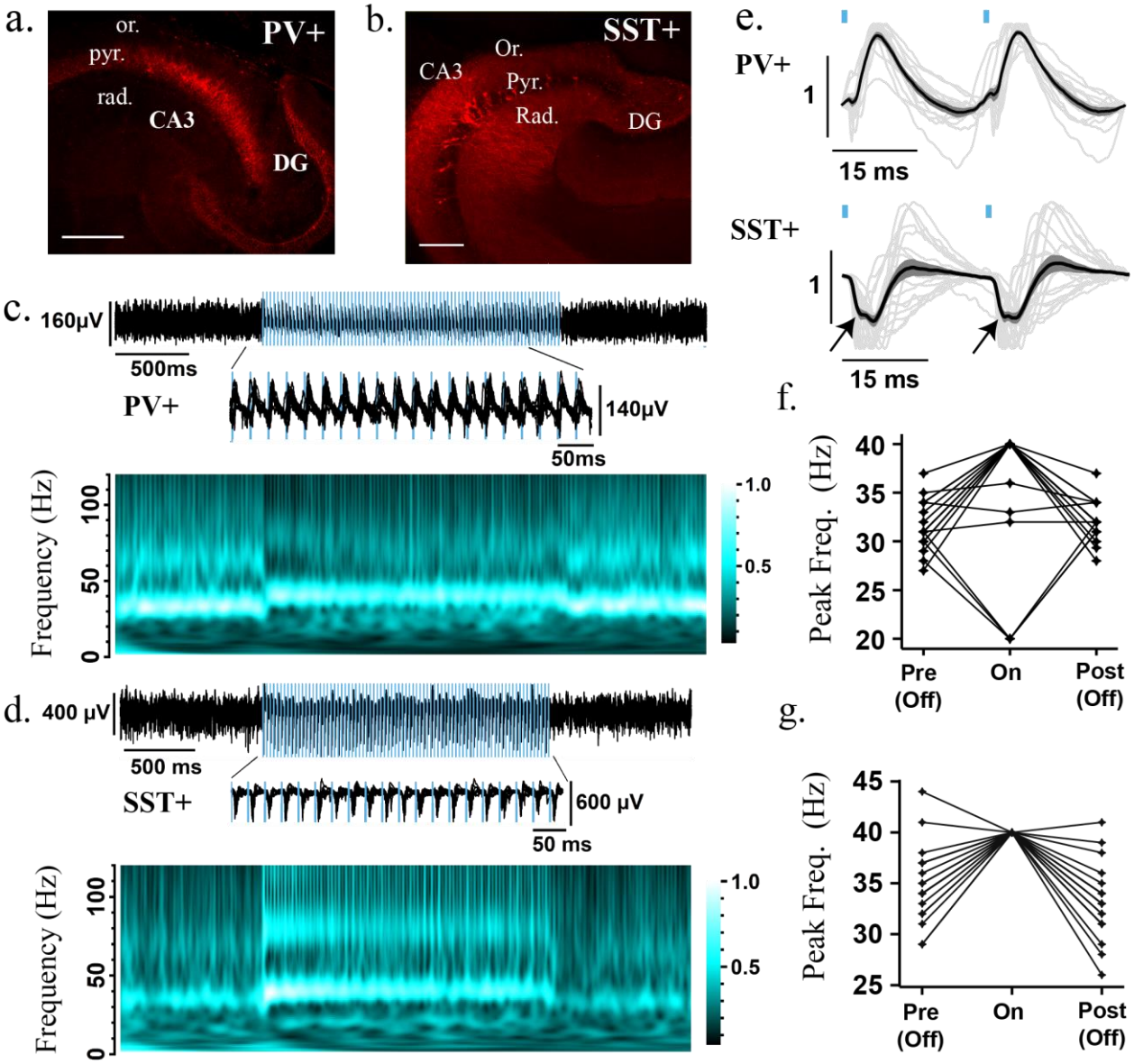

Figure 3: Rhythmic photo-stimulation of either PV+ or SST+ interneurons entrains Cch-induced gamma oscillations. Confocal image of ventral hippocampus (350 μm slice) from a: PV-cre mice and b: SST-cre mice with mCherry-ChR2 expression. CA3 = Cornu Ammonis 3, DG = Dentate Gyrus, Pyr. = stratum Pyramidale, Rad. = stratum Radiatum, Or. = Stratum Oriens. Scale bar = 200 μm. c and d) Top: Representative LFP recording from CA3 area illustrating the entrainment of Cch-induced oscillations to 40 Hz light pulses in c: PV-cre and d: SST-cre mice expressing mCherry-ChR2 (1ms pulse width; blue light illumination at 5.5 mW). Middle: Zoomed recordings during pulse stimulation. Bottom: Magnitude component of the wavelet transform normalised by its maximum value. Brighter colours represent larger gamma power. e) Normalised average waveform following two consecutive pulses at 40 Hz and 1 ms pulse width from each experiment (PV+: n = 15/18; SST+: n = 19/22). Black line is the population average, grey lines represent individual experiments and dark-grey shaded area is the SEM Black. Arrows indicate initial negative peak. f, g) Peak frequency of oscillation before (Pre (Off)), during (On) and after (Post (Off)) light stimulation in f: PV+ (n = 18/18) and g: SST+ (n = 19/22) experiments (note experiments entrained at 20 Hz reflect suppression of alternate gamma cycle – see suppl. Fig. 3aii). Black lines represent single experiments.

206

207

Supplementary Figure 3 (Supporting Figure 3)

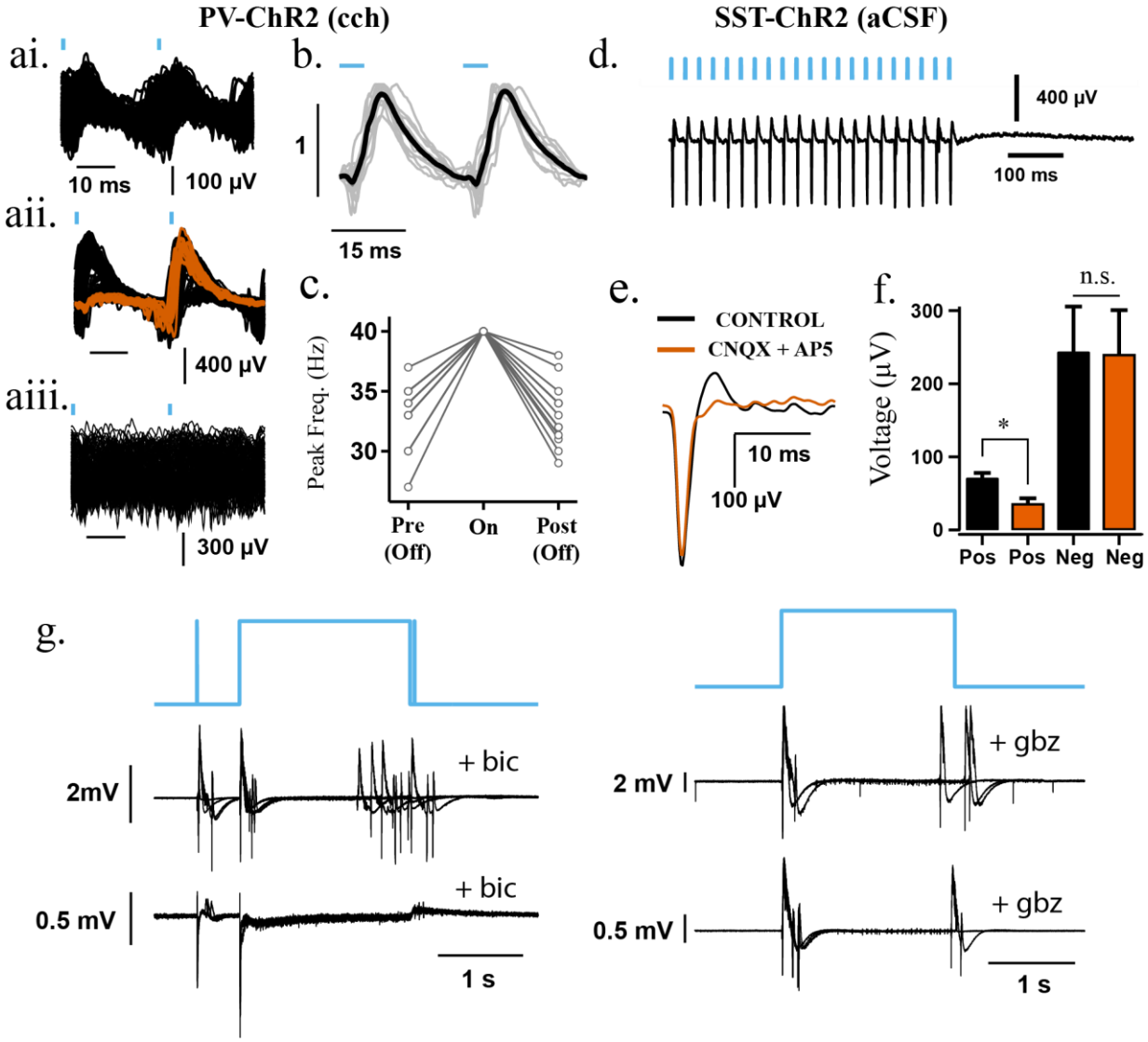

Supplementary Figure 3: a-c) Responses to pulse stimulation in slices with Cch-induced gamma oscillations from PV-ChR2 mice. a) Extracted waveforms following two consecutive pulses at 40 Hz (1 ms) from one experiment showing i) strong entrainment, ii) entrainment of half of the cycles and inhibition of the other half, and iii) no entrainment. Coloured lines represent a subset of extracted waveforms. b) Average waveform following two consecutive pulses at 40 Hz with pulse widths of 5 ms (n = 13/13). Black line is the population average, grey lines represent individual experiments and dark-grey/error bars shaded area is the SEM. c) Peak frequency of oscillation before (Pre (Off)), during (On) and after (Post (Off)) light stimulation at 40 Hz with pulse widths 5 ms (n = 13/13). Note that the slices with 20 Hz induction were not tested with 5 ms pulse width. d-g) Responses to pulse stimulation in slices from SST-ChR2 mice without cholinergic activation (aCSF). d) Representative LFP recording from CA3 area illustrating field responses during 40 Hz light pulses in the absence of Cch (1ms pulse width- 5.5 mW). e) Average waveform obtained with 1 ms pulse width at 40 Hz from one experiment before (black line) and after application of 20 µM CNQX and 40 µM AP5. In one experiment only 20 µM CNQX was applied but exhibited the same effect. f) The magnitude of negative and positive peaks before and after iGluR blocker application (n = 4). iGluR blockers used: 20 µM CNQX, 40 µM AP5, n = 3; 20 µM CNQX, n = 1. Positive peak before (MaxC) and after drug (MaxD) application ($t = 3.49$, $p = 0.03$, paired t-test). Negative peak before (MinC) and after drug (MinD) application ($t = -0.61$, $p = 0.58$, paired t-test). *$p < 0.05$, n.s. $p >= 0.05$. g) Induction of epileptiform bursts during photo-stimulation of SST+ interneurons following $GABA_AR$ blockage (n = 2 at 20 µM bicuculine (bic), n = 2 at 10 µM gabzine (gbz)).

Sustained activation of PV+ interneurons suppresses Cch-induced gamma oscillations

We used two patterns of sustained activation, light steps and fully-modulation sine waves at 8 Hz, and tested these in slices from PV-ChR2 mice. In a subset of light step experiments, we recorded ongoing gamma oscillations in the LFP whilst tonically driving PV+ interneurons at increasing strengths across trials (by changing the levels of blue light illumination, 10 - 5500 µW). The change in power between baseline and light activation period was measured at each light intensity level. We then obtained the response level at which the power changed by half of the maximum for each experiment (half-maximal response). For half-maximal response trials, photo-activation of PV+ interneurons (2 seconds) consistently decreased the power-area (0.52 +/- 0.016 compared to baseline, $t = -29.56$, $p < 0.01$, one-sample t-test; Fig. 4a-c, e) and increased the peak frequency (from 32.70 +/- 0.793 Hz (baseline) to 38.76 +/- 1.094 Hz, $t = 8.21$, $p < 0.01$, paired t-test; Fig. 4d, f). Furthermore, there was a progressive decrease in power ($r = -0.84$, $n = 121$ values, $t = 17.00$, $p < 0.01$) and increase in frequency ($r = 0.49$, $n = 100/121$values, $t = 5.60$, $p < 0.01$) as the light intensity increased (Fig. 4g-h). In order to estimate the maximal effect of PV+ interneuron stimulation, we pooled experiments using strong light intensity illumination (> 2mW, including cases where light intensity-response curves were not assessed; n = 14 at 5.5 mW, n = 9 at 2.2 mW). Overall, strong light illumination caused a substantial decrease in the normalised power-area (0.09 +/- 0.029, $t = 31.07$ $p < 0.01$, one-sample t-test; Fig. 4i, j) and abolished the oscillations in most experiments (17/23). These results indicate that progressive up-regulation of PV+ interneuron activity decreases gamma power and increases the frequency until the rest of the hippocampal network is fully silenced.

Interneurons have been shown to be particularly susceptible to depolarisation block (Herman *et al.*, 2014). In order to ensure that these effects were not caused from impaired action potential

generation in PV+ interneurons (i.e. depolarisation block), as we recorded spiking activity using a linear multi-electrode array (MEA) during Cch-induced oscillations. PV+ interneurons (spike width: 0.49 +/- 0.04 ms) maintained spiking activity during sustained illumination (5.5 mW; Median sustained activation index [IQR] = 0.87 [0.46, 1], Z=171, p<0.001, n=18, one-sample Wilcoxon signed rank test; analysis performed on last second of trial), and this was associated with decreased activity of regular spiking (RS; -0.72 [-0.92, -0.40]; Z=2, p<0.001, n=53, one-sample Wilcoxon signed rank test; z=65.7, p<0.001 cf. PV+ interneurons, Kruskal-Wallis Test followed by posthoc Dunn's test with Bonferroni correction for multiple comparisons) and fast-spiking cells (FS; -0.52 [-0.82, -0.12]; Z=141 p<0.001, n=49, one-sample Wilcoxon signed rank test; z=50.1, p<0.001 cf. PV+ interneurons, Kruskal-Wallis Test followed by posthoc Dunn's test with Bonferroni correction for multiple comparisons) (Supplementary Fig.4). These results are consistent with increased PV+ interneuron activity during light illumination that leads to reduced activity in hippocampal principal cells.

During 8 Hz sinusoidal modulation of PV+ interneurons, the instantaneous gamma magnitude, assessed using the Hilbert transform, was found to be negatively correlated with light intensity in agreement to light step experiments (across all experiments, Pearson correlation, mean r = -0.51 +/- 0.04, $t > 23.2$, $p < 0.01$, $n = 12$) (Suppl. Fig.4d). During MEA recordings, spike rates of PV+ interneurons correlated positively with theta-frequency changes in light intensity (Median rank correlation coefficient [IQR] = 0.75 [0.55, 0.83], Z=120, p=0.001, n=15, one-sample Wilcoxon signed rank test), while negative correlations were found for the spike rates of RS (-0.19 [-0.37, -0.09]; Z=100, p<0.001, n=43, one-sample Wilcoxon signed rank test; z=48.3, p<0.001 cf. PV+ interneurons, Kruskal-Wallis Test followed by posthoc Dunn's test with Bonferroni correction for multiple comparisons) and FS cells (-0.19 [-0.39, -0.01]; Z=232, p=0.006, n=42, one-sample Wilcoxon signed rank test; z=45.7, p<0.001 cf. PV+ interneurons, Kruskal-Wallis Test followed by posthoc Dunn's test with Bonferroni correction for multiple comparisons). These findings indicate that a transient

256 increase in PV+ interneuron activity causes a rapid and reversible decrease in the power of the Cch-

257 gamma oscillations and firing rates of other neurons.

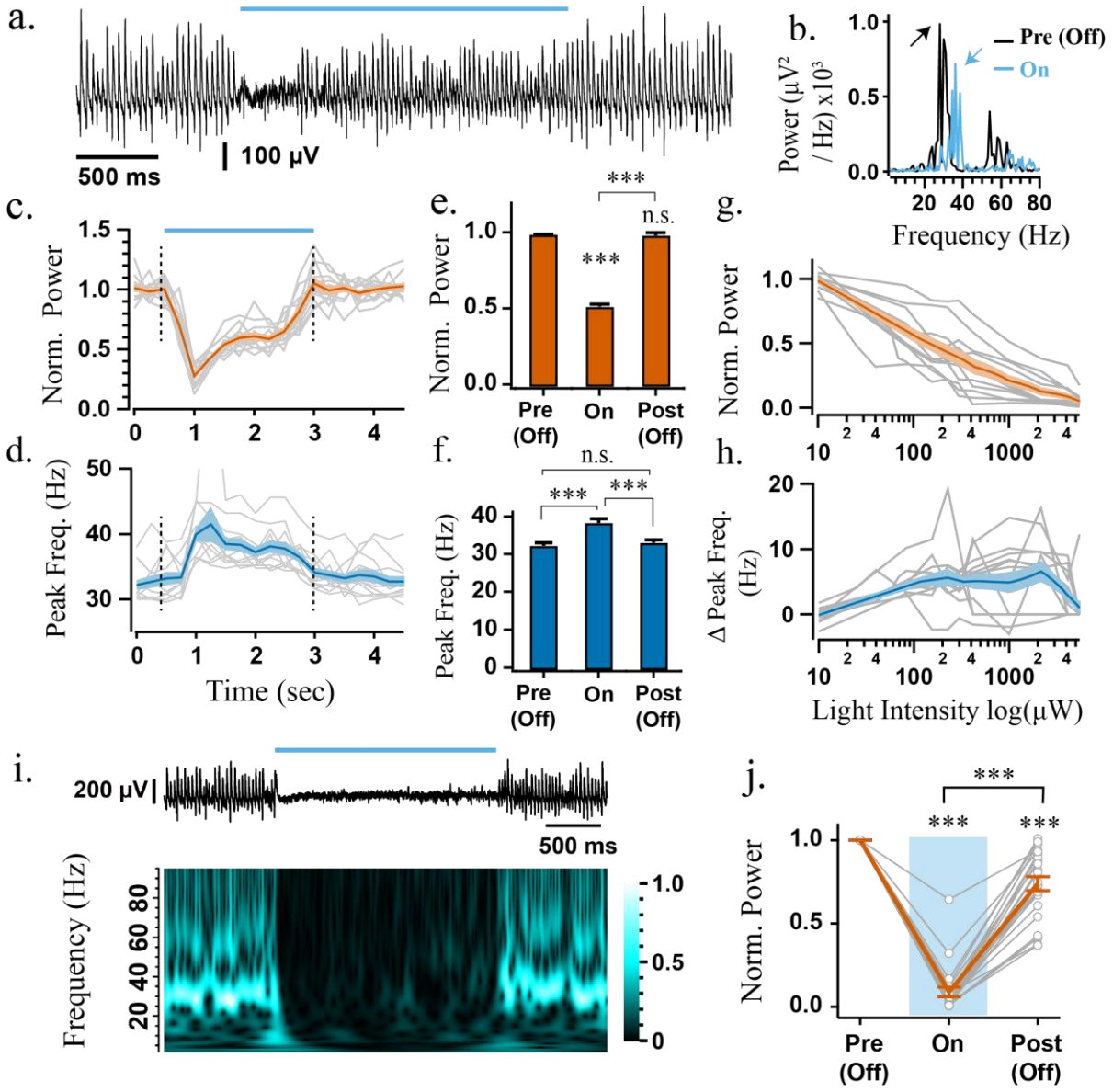

Figure 4: Sustained photo-excitation of PV+ interneurons decreases the power and increases the frequency of Cch-induced gamma oscillations. a) Representative LFP recordings from CA3 area illustrating effect of PV+ interneurons photo-excitation (155 µW) on gamma oscillations along with b) its respective power spectrum (arrows indicate power spectrum peaks). c) Power-area normalised to baseline and d) peak frequency of the oscillation calculated in 0.5 second bins across experiments (n = 12). e) Average change in power-area during (On) and after light stimulation (Post (Off)) normalised to baseline (Pre (Off)). f) Average peak frequency; rmANOVA: $F(1.14, 12.50) = 44.14$, $p < 0.001$. g) Power-area change and h) frequency difference between light stimulation period and baseline plotted against light intensity (n = 12). i) Top: Representative LFP recording from CA3 area illustrating the collapse of Cch-induced oscillations in response to strong and sustained blue light illumination (5.5 mW). Bottom: Magnitude component of the wavelet transform normalised by its maximum value. j) Average change in power-area upon strong and sustained blue light illumination (n total = 23 >2mW: n = 14 at 5.5 mW and n = 9 at 2.2 mW). Changes in peak frequency were analysed using rmANOVA, followed by post-hoc paired t-tests with correction for multiple comparisons. *p < 0.05, **p < 0.01, ***p < 0.001, n.s. p >= 0.05. Solid brackets represent paired t-tests and standalone star symbols represent one-sample t-test versus normalised baseline. Grey lines represent single experiments, error bars and shaded area are SEM and coloured line the population average.

259

Supplementary Figure 4 (Supporting Figure 4)

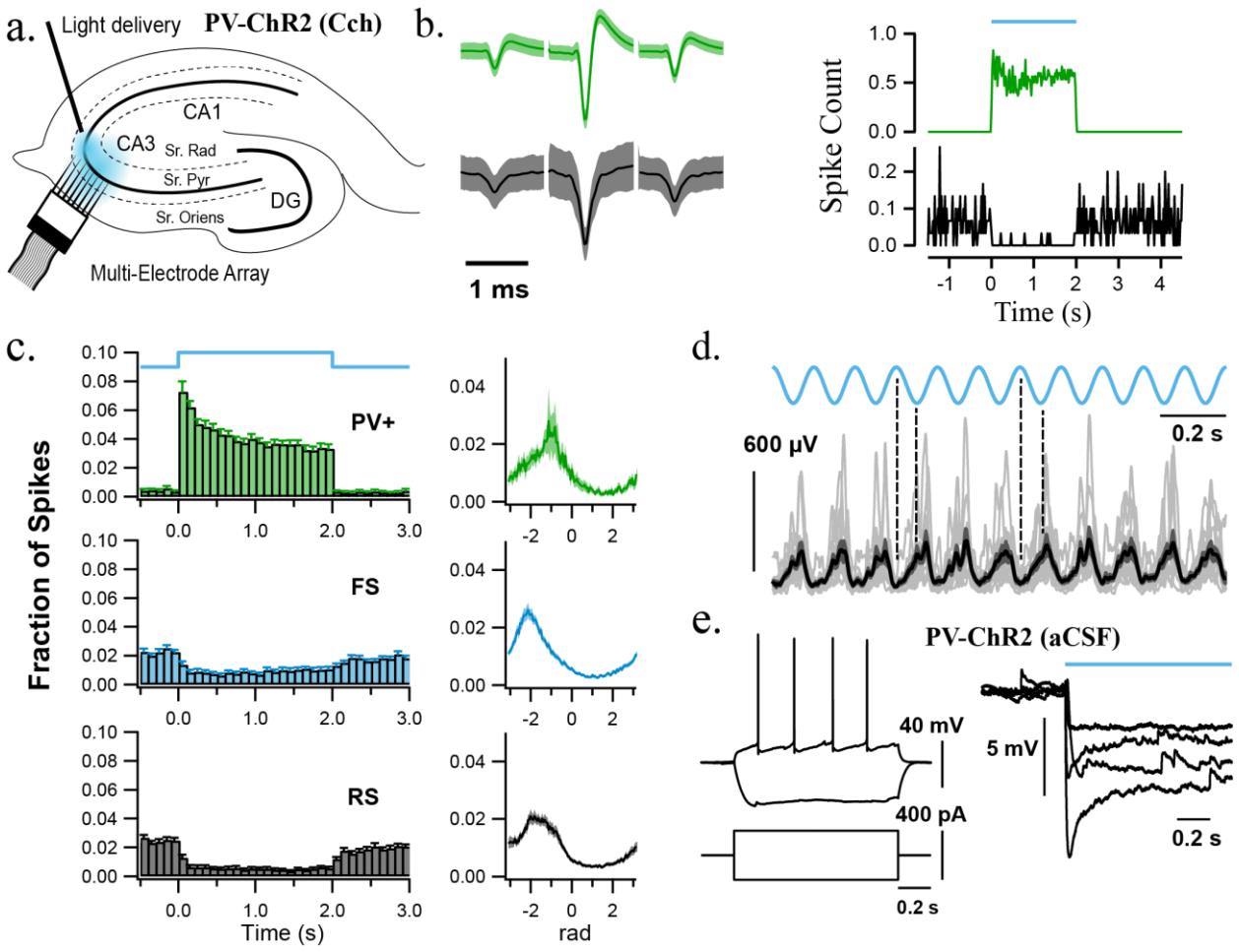

Supplementary Figure 4 (a-c): Multi-unit recordings during PV+ interneuron sustained photo-excitation in hippocampal slices with Cch-induced gamma oscillations. a) Schematic diagram of the hippocampus illustrating MEA recordings during blue light illumination (5.5 mW) in CA3. b) Left - Representative average spike waveforms, Right – spike histograms during sustained light illumination. (green FS single units, black RS multi-unit). c) Mean spike time histograms (left) and spike phase histograms (right) of photo-tagged PV+, FS and RS cells. Shaded regions represent standard deviation. The PV+ interneurons fired at a significantly later phase of the oscillation than the RS cells ($F(2,55) = 5.36$, $p = 0.007$, Two-sample Hotelling test). d) Instantaneous amplitude of the Hilbert transform during theta photo-activation (1 mW) overlaid across experiments (grey traces, n = 12), black represents the mean and dark grey the SEM. Dotted lines illustrate that high light intensity decreased gamma power. e) Intracellular recordings from pyramidal cells in aCSF, showing responses to current steps (left) and hyperpolarisation in response to PV+ interneuron photo-activation (n = 4).

Sustained activation of SST+ interneurons induces fast gamma oscillations

We obtained the light intensity response curves with light steps in slices from SST-ChR2 mice and observed similar results as in PV-ChR2 experiments. Sustained light illumination decreased the power (0.49 +/- 0.029, t = 17.53, p < 0.01, one sample t-test; Fig. 5a-c, e) and increased the frequency at half-maximal response (from 34.08 +/- 0.954 Hz during baseline period to 38.17 +/- 1.400 Hz, t = 3.658, p = 0.011, paired t-test; Fig. 5d, f). Moreover, as the light intensity increased, the power progressively decreased (r = -0.66, n = 107 values, t = 9.11, p < 0.01; Fig. 5g), and frequency progressively increased (r = 0.71, n = 56 out of 107 values, t = 7.41, p < 0.01; Fig. 5h). It is perhaps not surprising that excitatory networks can be suppressed by photo-activation of GABAergic interneurons. However, different responses were revealed when we assessed the effects of strong photo-activation of SST+ interneurons on Cch-induced gamma oscillations (light-intensity response curves where performed in a subset of experiments; n = 18 slices at 5.5 mW and n = 13 slices at 2.2 mW, merged). Consistent with PV-ChR2 step experiments, the gamma power was reduced during light stimulation when compared to baseline period (0.34 +/- 0.150, t = -4.39, p < 0.01, one sample t-test; Fig. 4.6b) and in approximately half of the experiments, gamma oscillations were fully abolished (n = 16/31 slices). In contrast, in experiments where the oscillations persisted, their frequency increased strongly from 34.63 +/- 0.836 Hz during baseline to 62.75 +/- 4.921 Hz during light illumination (n = 15/31 slices; t =5.61, p < 0.01, paired t-test; Fig 5i-k). These fast gamma oscillations occurred most reliably in slices that the light-intensity response curves were not obtained. In order to test if SST+ interneuron photo-activation alone is sufficient to induce oscillations, as opposed to simply increasing the frequency of ongoing activity, we repeated the same experiments in the absence of Cch. Sustained photo-activation of SST+ interneurons induced *de novo* oscillations in the fast gamma-band range with peak frequency of 80.5 +/- 2.48 Hz (12/16

284 slices; Fig. 6a, c). Isolating the CA3 area from DG did not prevent the generation of *de novo*
285 oscillations (n = 3 slices).

286 Furthermore, sinusoidal light activation at 8 Hz (theta photo-activation) also induced robust
287 oscillations with higher peak frequency than the tonic activation 111.2 +/- 3.15 Hz (13/17 slices; t =
288 7.64, $p < 0.001$, two-sample t-test; Fig. 6b, d-e). This is consistent with previous experiments
289 showing that transient light activation induces higher frequency oscillations than sustained
290 illumination (Butler *et al.*, 2016; Betterton *et al.*, 2017). Furthermore, the power ($r = 0.67$, n = 70
291 values, $t = 7.52$ $p < 0.01$) and frequency ($r = 0.77$, n = 48/70 values, $t = 8.20$, $p < 0.01$) of the *de novo*
292 oscillations progressively increased as the light intensity of theta photo-activation was elevated (Fig.
293 6f). This monotonic increase in peak frequency contrasts with the properties of oscillations induced
294 by photo-activation of principal cells in the hippocampus, where the frequency of the oscillations
295 remains relatively constant within the slow gamma band across light intensities (Butler *et al.*, 2016;
296 Betterton *et al.*, 2017; Butler, Hay & Paulsen, 2018). Therefore, SST+ interneuron photo-activation
297 in CA3 appears to induce a distinct type of gamma activity.

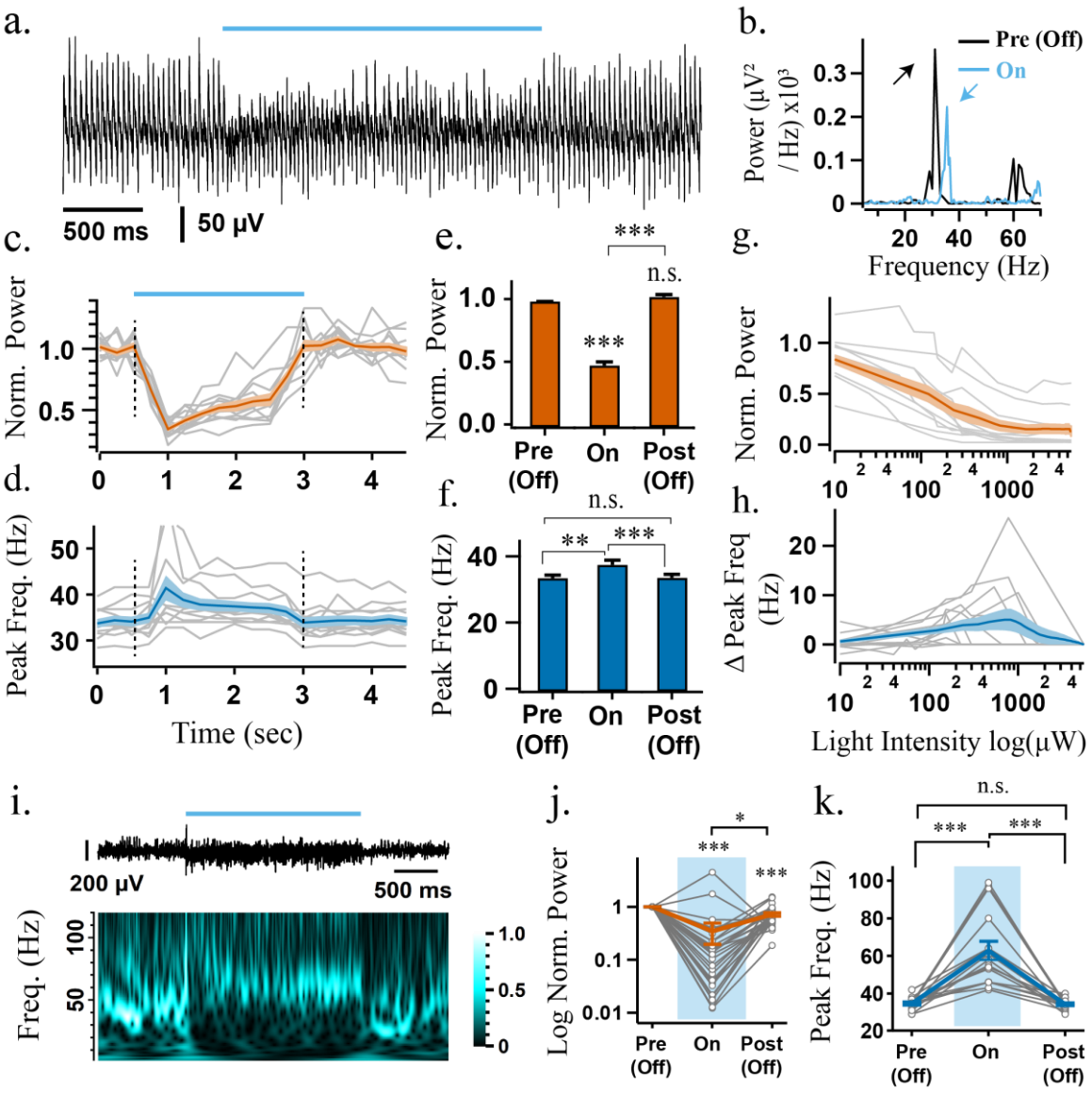

Figure 5: Sustained photo-excitation of SST+ interneurons decreases the power and increases the frequency of Cch-induced gamma oscillations but can also induce high-frequency oscillations. a) Representative LFP recordings from CA3 area illustrating effect of SST+ interneurons photo-excitation (155 µW) on gamma oscillations along with b) its respective power spectrum (arrows indicate power spectrum peaks). c) Power-area normalised to baseline and d) peak frequency of the oscillation calculated in 0.5 second bins across experiments (n = 12). e) Average change in power-area during (On) and after light stimulation (Post (Off)) normalised to baseline (Pre (Off)). f) Average peak frequency; rmANOVA: $F(1.05, 11.59) = 15.05$, $p = 0.002$. g) Power-area change and h) frequency difference between light stimulation period and baseline plotted against light intensity (n = 12). i) Top: Representative LFP recording from CA3 area illustrating the induction of high-frequency oscillations in response to strong and sustained blue light illumination (5.5 mW). Bottom: Magnitude component of the wavelet transform normalised by its maximum value. j) Normalised power of Cch-oscillations during SST+ interneurons cell photo-activation (n = 31). k) Peak frequency of oscillations that were not abolished from strong light illumination (n remaining = 16/31: n = 4 at 5.5 mW and n = 12 at 2.2 mW); rmANOVA: $F(1.03, 15.39) = 31.45$, $p < 0.001$. Changes in peak frequency were analysed using rmANOVA, followed by post-hoc paired t-tests with correction for multiple comparisons. *p < 0.05, **p < 0.01, ***p < 0.001, n.s. p >= 0.05. Solid brackets represent paired t-tests and standalone star symbols represent one-sample t-test versus normalised baseline. Grey lines represent single experiments, error bars and shaded area are SEM and coloured line the population average.

The fast gamma oscillations that emerge during sustained photo-activation of SST+ interneurons could reflect the intrinsic synchronisation of SST+ networks, but there are a number of possible scenarios in which this stimulation paradigm could lead to the activation of other hippocampal microcircuits involving network excitation. Depolarising GABA could contribute to recruitment of postsynaptic targets, but perforated patch recordings from hippocampal cells in stratum pyramidale (aCSF only) showed that they were hyperpolarized by light illumination (Supplementary Fig. 5f-g). Alternatively, network excitation and oscillogenesis could emerge following depolarisation block of SST+ interneurons, and subsequent disinhibition, but direct photo-inhibition of SST+ interneurons was not able to generate *de novo* oscillations (Supplementary Fig. 5a-b). However, the power of the light-induced oscillations was markedly reduced following block of either fast excitation or inhibition, and whole cell recordings in putative principal cells indicated that they received weak excitatory postsynaptic currents (EPSCs) throughout light illumination (Supplementary Fig. 5c-e, h-j). This suggests that the light-induced oscillations recorded in LFP do not emerge solely from the activity of SST+ interneurons.

To directly test if photo-excitation of SST+ interneurons leads to a dominant effect of depolarisation block during ongoing gamma oscillations, and whether photo-excitation is associated with net increases or decreases in the spiking activity of other neurons in the network, we performed MEA recordings. We found that SST+ interneurons (spike width: 0.69 +/- 0.03 ms) displayed increased activity throughout the course of step stimulation (Median sustained activation index [IQR] = 0.90 [0.76, 0.98], Z=2346, p<0.001, n=68, one-sample Wilcoxon signed rank test; Fig. 6j-top), and faithfully followed the 8 Hz sine stimulation (Median rank correlation coefficient [IQR] = 0.63 [0.52, 0.72], Z=1484, P<0.001, n=54, one-sample Wilcoxon signed rank test; Fig. 6j-middle). All but 3 of the SST+ interneurons recorded were significantly phase-coupled to the induced fast gamma-frequency oscillations (p<0.05, Rayleigh test), with a mean spike phase of -2.0 [-2.1, -1.8] radians (second-order mean [95% confidence intervals]; n=65; Fig. 6j-bottom). The RS and FS cells showed significantly

weaker modulation (Fig. 6j), but did not appear to be suppressed as in the PV-ChR2 experiments, and rather showed an insignificant trends towards both increased activity during step illumination (Median sustained activation index [IQR]; RS: 0.12 [-0.08, 0.54], Z=50, p=0.13, n=11; FS: 0.49 [-0.14, 0.59], Z=24, p=0.09, n=7; one-sample Wilcoxon signed rank tests) and positive correlations with theta-frequency changes in light intensity (Median rank correlation coefficient [IQR]; RS: 0.26 [-0.07, 0.53], Z=49, p=0.16, n=11; FS: 0.28 [0.09, 0.57] (Z=25, p=0.06, n=7, one-sample Wilcoxon signed rank tests). The majority of RS (8/11) and FS cells (4/7) were also significantly phase-coupled to the light-induced fast gamma oscillations ($p<0.05$, Rayleigh test), but did not show a consistent mean firing phase (RS: $F(2,8)=2.3$, $p=0.18$; FS: $F(2,2)=4.5$, $p=0.19$; parametric second-order analysis (Zar, 1999)). Overall, this suggests that the dominant change in the network during the induction of fast gamma oscillations is a robust increase in the spiking of SST+ interneurons.

To explore whether the recruitment of SST+ interneurons might differ between step and theta stimulation, we analysed the maximum spike rates in the second half of the stimulation trials (20 ms bins). The maximum spike rates during theta stimulation were significantly higher than during the step stimulation ($Z=148$, $p<0.001$, $n=54$; Wilcoxon signed rank test). As theta stimulation induced faster gamma oscillations than step stimulation (see Fig. 6e), this further suggests that the frequency of fast gamma oscillations depends on the overall levels of SST+ interneuron excitation.

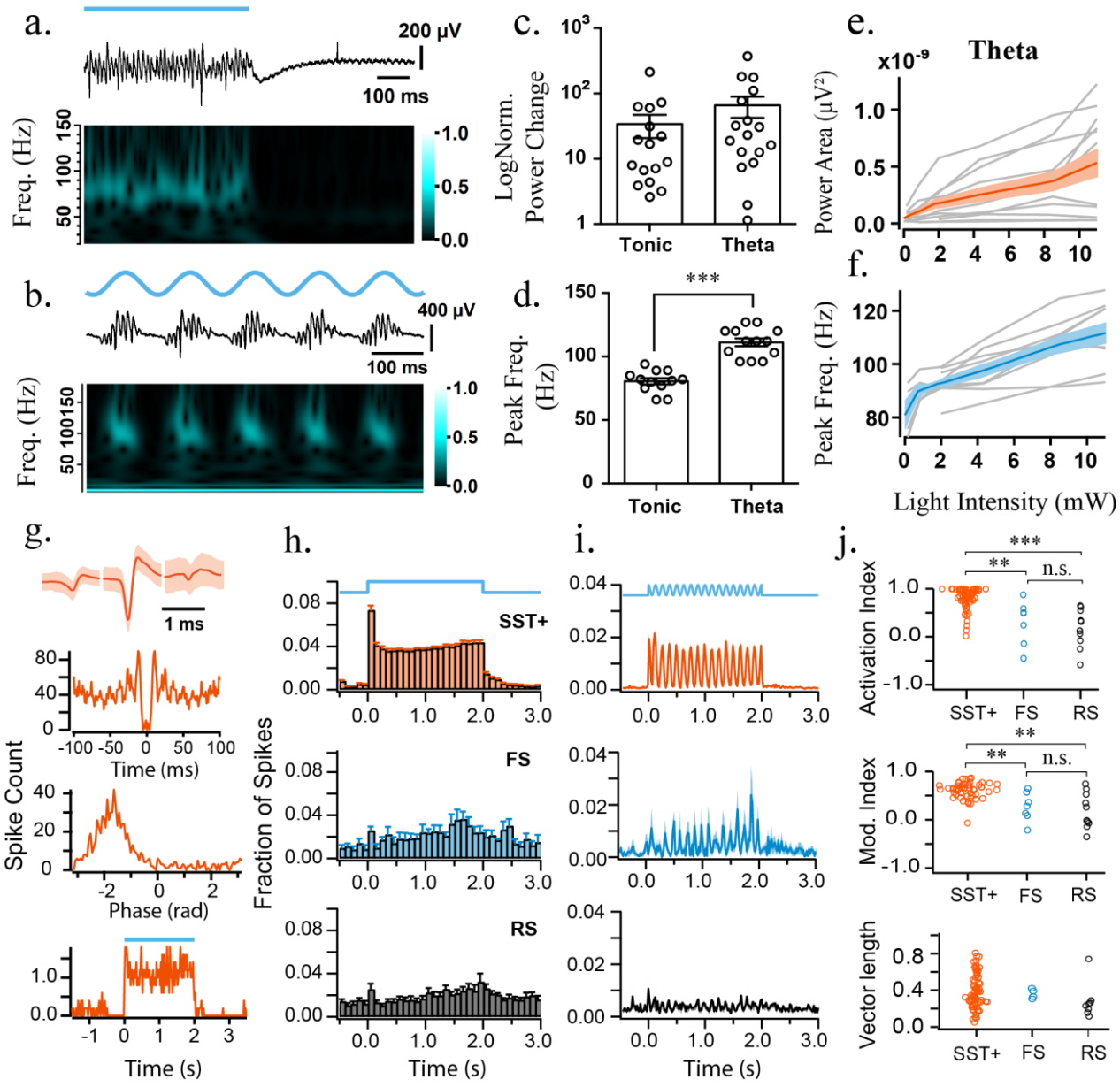

Figure 6: Photo-activation of SST+ interneurons induces *de novo* oscillations in the absence of Cch. a, b) Top: Representative LFP recording from CA3 area illustrating induction of high-frequency oscillations by a) constant and b) theta blue light illumination (10 mW). Bottom: Magnitude component of the wavelet transform normalised by its maximum value; brighter colours represent larger magnitude. c) Log power change compared to baseline during constant (n = 16) and theta blue light illumination (n = 17). d) Peak frequency of the *de novo* oscillations is higher when induced by theta when compared to tonic stimulation; two-sample t-test, ***p < 0.001. Grey lines/markers represent single experiments, black line is the population average and error bars are the SEM. e) Power-area and f) frequency during light stimulation period plotted against light intensity of theta photo-activation (n = 12). The black line is the average response and the dark-grey shaded area represents SEM. (g-i) Multi-unit recordings during SST+ interneuron sustained photo-excitation g) Putative opto-tagged SST+ average spike waveform, autocorrelation, phase and step histogram during sustained light illumination. h) step histogram, i) sinusoidal histogram of photo-tagged SST+, FS and RS cells. Shaded regions represent standard deviation. j) top to bottom: sustained activation index, modulation index and vector length. Kruskal-Wallis Test was followed by posthoc Dunn's test with Bonferroni correction for multiple comparisons. *p < 0.05, **p < 0.01, ***p < 0.001, n.s. p >= 0.05.

342

Supplementary figure 5 (Supporting figure 6)

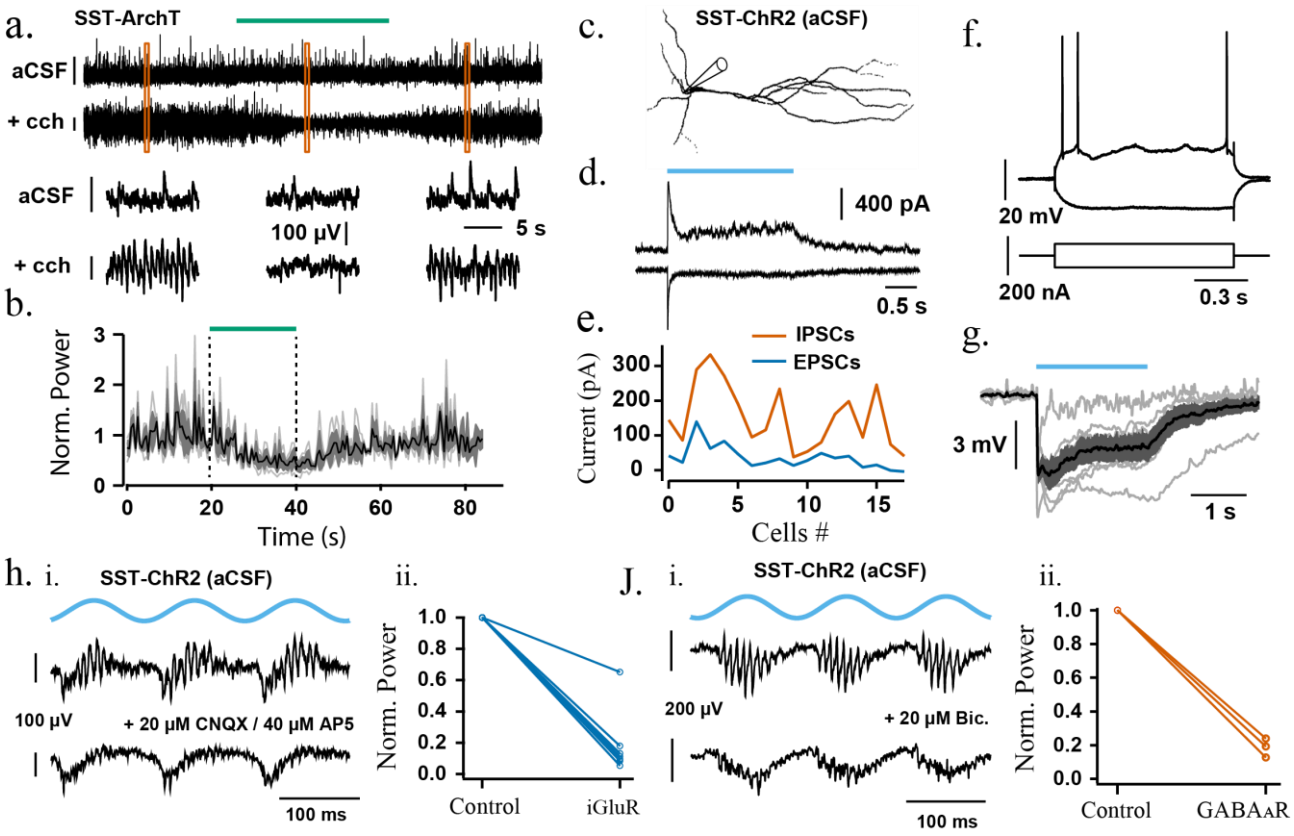

Supplementary Figure 5: (a–b) Responses to laser illumination in SST-cre mice expressing ArchT-GFP. a) Representative LFP recording with and without the presence of Cch during green laser illumination (approx. 18.6 mW). Orange squares represent the bottom sections of LFP that were magnified. b) Change in power-area normalised to baseline calculated in 1 second bins across experiments (n = 3) in the absence of Cch; Dotted lines indicate the duration of laser illumination. (c-e) Voltage clamp recordings from putative pyramidal cells during photo-activation of SST+ interneurons (1.53 mW). c) Reconstruction of a recorded cell with typical pyramidal cell morphology in CA3 hippocampal area. d) Representative voltage clamp recording of the cell in c) held at 0 mV (top) and -70mV (bottom) to isolate IPSCs and EPSCs, respectively. e) Comparison of EPSCs and IPSCs during SST+ interneuron photo-activation across cells (n = 18). Blue line = EPSCs, Orange line = IPSCs. (f–g) Perforated patch recordings in CA3 pyramidal cell layer in SST-cre mice expressing ChR2-mcherry. f) Current clamp recording in a putative pyramidal cell in response to depolarising and hyperpolarising current injections. g) Hyperpolarisation of the membrane voltage of perforated patched cells (n = 6) during blue light illumination (1.53 mW). Grey traces represent individual cells, black trace the average and dark grey shaded area the SEM. (h-j) pharmacology of de-novo oscillations induced by sinusoidal blue light illumination in SST-cre mice expressing ChR2-mcherry (1 - 10 mW). Representative LFP recording in CA3 before (top) and after (bottom) application of h.i) iGLUR blockers and j.i) $GABA_AR$ blockers. Power-area change before (control) and after application h.ii) iGLUR blockers and j.ii) $GABA_AR$ blockers. GluR blockers used: 20 µM CNQX, 40 µM AP5, n = 3; 10 µM CNQX, 20 µM AP5, n = 1; 20 µM CNQX, n = 1; 3mM kynurenic, n = 3. $GABA_AR$ blockers: 20 µM Bicuculline, n = 2; 20 µM Gabazine, n = 1.

Discussion

Gamma oscillations depend on synchronised synaptic inhibition, and there is a wealth of evidence suggesting that perisomatic-targeting PV+ interneurons provide the critical inhibitory output for both current and rhythm generation (Mann *et al.*, 2005; Bartos, Vida & Jonas, 2007; Oren, Hájos & Paulsen, 2010; Tukker *et al.*, 2013; Cardin, 2016; Sohal, 2016; Penttonen *et al.*, 1998b). Here, we used optogenetic manipulation of PV+ and SST+ interneurons to explore whether PV+ interneurons have a selective role in gamma rhythmogenesis in the hippocampal CA3 *ex vivo*. Our findings suggest that optogenetically disrupting interneuronal activity, via either photo-inhibition or photo-excitation, generally leads to a decrease in the power and increase in the frequency of ongoing cholinergically-induced slow gamma oscillations. This suggests that both PV+ and SST+ interneurons play key roles in maintaining slow gamma oscillations, and the key differences were that (i) cholinergically-induced gamma oscillations were more readily disrupted by photo-inhibition of SST+ interneurons rather than PV+ interneurons, (ii) manipulation of SST+ interneurons modulated gamma oscillation frequency more robustly than that of PV+ interneurons, and (iii) photo-stimulation of SST+ interneurons could also induce *de novo* fast gamma oscillations.

Slow gamma oscillations in the hippocampal CA3 appear to be generated by synaptic feedback loops between excitatory pyramidal neurons and perisomatic-targeting interneurons, both in brain slices (Fisahn *et al.*, 1998; Hajos, 2004; Mann *et al.*, 2005; Oren *et al.*, 2006; Butler, Hay & Paulsen, 2018) and *in vivo* (Bragin *et al.*, 1995; Csicsvari *et al.*, 2003; Fuchs *et al.*, 2007). In such feedback loops, the period of the oscillation largely reflects the effective time course of inhibitory postsynaptic potentials in the pyramidal cells, which should become shorter with smaller compound inhibitory synaptic currents and/or increased pyramidal cell excitability. The amplitude of the oscillation recorded in the LFP also reflects the amplitude of phasic inhibitory currents in pyramidal neurons (Mann *et al.*, 2005; Oren, Hájos & Paulsen, 2010), and during spontaneous gamma oscillations there

367 is a strong correlation between the instantaneous period and amplitude of each gamma cycle
368 (Atallah & Scanziani, 2009). One might thus expect disinhibition to decrease the amplitude and
369 increase the frequency of gamma oscillations, which is largely what we observed with photo-
370 inhibition of either PV+ or SST+ interneurons. Observing similar effects with photo-stimulation of
371 interneurons might be somewhat more surprising. However, our interpretation is that this also
372 effectively disrupts synchronisation within synaptic feedback loops, by silencing a subpopulation of
373 pyramidal cells and thus 'knocking out' part of the gamma oscillating network. In both types of
374 optogenetic manipulation, we could thus be recording the activity in residual parts of the network
375 that can maintain synaptic feedback loops, albeit with weaker synchronised inhibition.

376 While photoinhibition of either PV+ or SST+ interneurons was able to disrupt cholinergically-induced
377 gamma oscillations, it was necessary to use high-powered laser illumination of PV+ interneurons to
378 consistently reduce gamma power, and the oscillations were not abolished under our stimulation
379 paradigms. This is not inconsistent with PV+ interneurons playing a key role in the synaptic feedback
380 loops generating gamma oscillations in the hippocampal CA3, as such a microcircuit should resist
381 disinhibition. Indeed, strong laser illumination was necessary to biochemically silence PV+
382 interneuron terminals (El-Gaby *et al.*, 2016), and thus break this feedback loop. The lack of
383 consistent effects on the frequency of cholinergically-induced gamma oscillations may also be due
384 to the difficulty in silencing PV+ interneurons. Alternatively, it is possible that the remaining PV+
385 interneurons take longer to fire in each gamma cycle due to the Arch-induced hyperpolarisation.
386 Combined with a more excitable pyramidal neurons, which recover more rapidly form synaptic
387 inhibition, this could leave the overall oscillation frequency unchanged.

388 It was recently suggested that SST+ interneurons, but not PV+ interneurons, contribute to the
389 generation of slow gamma oscillations in V1 (Chen *et al.*, 2017; Veit *et al.*, 2017; Hakim, Shamardani
390 & Adesnik, 2018). Our results do not support an exclusive role for SST+ interneurons in slow

391 hippocampal gamma oscillations, but are consistent with an important role for SST+ interneurons
392 in gamma rhythmogenesis across cortical circuits. However, SST+ interneurons largely target the
393 dendritic domains of pyramidal cells, and thus it remains difficult to see how they could directly
394 contribute to the precise timing of pyramidal cell spiking during fast brain oscillations, such as
395 cholinergically-induced gamma oscillations in hippocampal CA3. SST+ bistratified interneurons have
396 been proposed to have similar properties to fast spiking PV+ interneurons, and also form a small
397 portion of synapses close to the soma (Somogyi & Klausberger, 2005; Muller & Remy, 2014), but
398 have been reported to exhibit decreased GABA release under cholinergic stimulation (Gulyás *et al.*,
399 2010). It therefore seems likely that the importance of SST+ interneurons to the generation of
400 cholinergically-induced hippocampal gamma oscillations lies in their modulation of perisomatic
401 feedback loops, via effects on both pyramidal neuron excitability, and the spike rate and precision
402 in PV+ interneurons (Savanthrapadian *et al.*, 2014).

403 While optogenetic manipulation of SST+ interneurons consistently disrupted slow gamma
404 oscillations, we found that photo-stimulation of SST+ interneurons could also induce *de novo* fast
405 gamma oscillations. These GABAergic interneurons should provide a powerful source of circuit
406 inhibition (Somogyi & Klausberger, 2005; Pfeffer *et al.*, 2013; Taniguchi *et al.*, 2011; Leão *et al.*, 2012;
407 Lovett-Barron *et al.*, 2012, 2014; Royer *et al.*, 2012; Urban-Ciecko & Barth, 2016), but we found that
408 sustained photo-stimulation of SST+ interneurons did not significantly inhibit the activity of STT-
409 neurons, and that pulsed stimulation could drive network excitation. It may be that the
410 hyperactivation of a dense plexus of SST+ processes in the dendritic layers leads to bystander effects
411 on nearby SST- neurons, possibly via ephaptic interactions and/or changes in the extracellular ionic
412 environment (Anastassiou *et al.*, 2011; Ferenczi *et al.*, 2016b), which counteracts the effects of
413 synaptic inhibition. The generation of fast gamma oscillations appeared to depend on the
414 maintenance of network excitability, as the oscillations were attenuated by block of iGluR. However,
415 the spiking of the majority of STT- RS neurons was only weakly coupled to the phase of light-induced

fast gamma oscillations, and without a consistent population spike phase preference, while light-sensitive putative SST+ interneurons showed reliable phase-locking. This could be consistent with fast gamma oscillations representing rhythmic dendritic inhibition from STT+ interneurons, with only weak effects on the spike rate and timing of other neurons in the network.

The mechanism by which a network of SST+ interneurons might generate fast gamma oscillations remains obscure. In neocortex, SST+ interneurons avoid inhibiting each other (Pfeffer *et al.*, 2013), although there is evidence for sparse synaptic interactions between SST+ interneurons in the hippocampus (Savanthrapadian *et al.*, 2014), and for more generic coupling via gap junctions (Baude *et al.*, 2007). More experiments are required to resolve the mechanisms by which optogenetic manipulation of interneurons influences hippocampal gamma oscillations, and whether STT+ neurons contribute to fast hippocampal gamma oscillations during theta and non-theta states *in vivo* (Sullivan *et al.*, 2011). However, our findings suggest that SST+ interneurons exert powerful control over the power and frequency of slow hippocampal gamma oscillations, and can switch the network between slow and fast gamma states.

REFERENCES

Akam, T. & Kullmann, D.M. (2010) Oscillations and Filtering Networks Support Flexible Routing of Information. *Neuron*. [Online] 67 (2), 308–320. Available from: doi:10.1016/j.neuron.2010.06.019.

Anastassiou, C.A., Perin, R., Markram, H. & Koch, C. (2011) Ephaptic coupling of cortical neurons. *Nature Neuroscience*. [Online] 14 (2), 217–223. Available from: doi:10.1038/nn.2727.

Andersen, P., Bliss, T.V.P. & Skrede, K.K. (1971) Unit analysis of hippocampal population spikes. *Experimental Brain Research*. [Online] 13 (2), 208–221. Available from: doi:10.1007/BF00234086.

Atallah, B. V. & Scanziani, M. (2009) Instantaneous Modulation of Gamma Oscillation Frequency by Balancing Excitation with Inhibition. *Neuron*. [Online] 62 (4), 566–577. Available from: doi:10.1016/J.NEURON.2009.04.027.

Bartos, M. & Elgueta, C. (2012) Functional characteristics of parvalbumin- and cholecystokinin-expressing basket cells. *The Journal of Physiology*. [Online] 590 (4), 669–681. Available from: doi:10.1113/jphysiol.2011.226175.

Bartos, M., Vida, I. & Jonas, P. (2007) Synaptic mechanisms of synchronized gamma oscillations in inhibitory interneuron networks. *Nature reviews. Neuroscience*. [Online] 8 (1), 45–56. Available from: doi:10.1038/nrn2044.

Basar-Eroglu, C., Brand, A., Hildebrandt, H., Karolina Kedzior, K., et al. (2007) Working memory related gamma oscillations in schizophrenia patients. *International Journal of Psychophysiology*. [Online] 64 (1), 39–45. Available from: doi:10.1016/j.ijpsycho.2006.07.007.

Bastos, A.M., Vezoli, J. & Fries, P. (2015) Communication through coherence with inter-areal

453 delays. *Current Opinion in Neurobiology*. [Online] 31, 173–180. Available from:
454 doi:10.1016/J.CONB.2014.11.001.

455 Baude, A., Bleasdale, C., Dalezios, Y., Somogyi, P., et al. (2007) Immunoreactivity for the GABAA
456 Receptor 1 Subunit, Somatostatin and Connexin36 Distinguishes Axoaxonic, Basket, and
457 Bistratified Interneurons of the Rat Hippocampus. *Cerebral Cortex*. [Online] 17 (9), 2094–
458 2107. Available from: doi:10.1093/cercor/bhl117.

459 Beierlein, M., Gibson, J.R. & Connors, B.W. (2000) A network of electrically coupled interneurons
460 drives synchronized inhibitionin neocortex. *Nature Neuroscience*. [Online] 3 (9), 904–910.
461 Available from: doi:10.1038/78809.

462 Betterton, R.T., Broad, L.M., Tsaneva-Atanasova, K. & Mellor, J.R. (2017) Acetylcholine modulates
463 gamma frequency oscillations in the hippocampus by activation of muscarinic M1 receptors
464 Panayiota Poirazi (ed.). *European Journal of Neuroscience*. [Online] 45 (12), 1570–1585.
465 Available from: doi:10.1111/ejn.13582.

466 Boyden, E.S., Zhang, F., Bamberg, E., Nagel, G., et al. (2005) Millisecond-timescale, genetically
467 targeted optical control of neural activity. *Nature Neuroscience*. [Online] 8 (9), 1263–1268.
468 Available from: doi:10.1038/nn1525.

469 Bragin, A., Jandó, G., Nádasdy, Z., Hetke, J., et al. (1995) Gamma (40-100 Hz) oscillation in the
470 hippocampus of the behaving rat. *The Journal of neuroscience : the official journal of the*
471 *Society for Neuroscience*. [Online] 15 (1 Pt 1), 47–60. Available from:
472 doi:https://doi.org/10.1523/JNEUROSCI.15-01-00047.1995.

473 Burns, S.P., Xing, D. & Shapley, R.M. (2011) Is gamma-band activity in the local field potential of V1
474 cortex a 'clock' or filtered noise? *The Journal of neuroscience : the official journal of the*
475 *Society for Neuroscience*. [Online] 31 (26), 9658–9664. Available from:

doi:10.1523/JNEUROSCI.0660-11.2011.

Butler, J.L., Hay, Y.A. & Paulsen, O. (2018) Comparison of three gamma oscillations in the mouse entorhinal-hippocampal system. *European Journal of Neuroscience*. [Online] Available from: doi:10.1111/ejn.13831.

Butler, J.L., Mendonça, P.R.. F., Robinson, H.P.C. & Paulsen, O. (2016) Intrinsic Cornu Ammonis Area 1 Theta-Nested Gamma Oscillations Induced by Optogenetic Theta Frequency Stimulation. *The Journal of neuroscience : the official journal of the Society for Neuroscience*. [Online] 36 (15), 4155–4169. Available from: doi:10.1523/JNEUROSCI.3150-15.2016.

Butler, J.L. & Paulsen, O. (2014) The Hippocampal Cacophony: Multiple Layers of Communication. *Neuron*. [Online] 84 (2), 251–253. Available from: doi:10.1016/J.NEURON.2014.10.017.

Buzsáki, G. & Wang, X.-J. (2012) Mechanisms of Gamma Oscillations. *Annual Review of Neuroscience*. [Online] 35 (1), 203–225. Available from: doi:10.1146/annurev-neuro-062111-150444.

Cardin, J.A. (2016) Snapshots of the Brain in Action: Local Circuit Operations through the Lens of γ Oscillations. *Journal of Neuroscience*. [Online] 36 (41), 10496–10504. Available from: doi:10.1523/JNEUROSCI.1021-16.2016.

Cardin, J.A., Carlén, M., Meletis, K., Knoblich, U., et al. (2009) Driving fast-spiking cells induces gamma rhythm and controls sensory responses. *Nature*. [Online] 459 (7247), 663–667. Available from: doi:10.1038/nature08002.

Chen, G., Zhang, Y., Li, X., Zhao, X., et al. (2017) Distinct Inhibitory Circuits Orchestrate Cortical beta and gamma Band Oscillations. *Neuron*. [Online] 96 (6), 1403–1418.e6. Available from: doi:10.1016/j.neuron.2017.11.033.

Chow, B.Y., Han, X., Dobry, A.S., Qian, X., et al. (2010) High-performance genetically targetable

optical neural silencing by light-driven proton pumps. *Nature*. [Online] 463 (7277), 98–102. Available from: doi:10.1038/nature08652.

Colgin, L.L., Denninger, T., Fyhn, M., Hafting, T., et al. (2009) Frequency of gamma oscillations routes flow of information in the hippocampus. *Nature*. [Online] 462 (7271), 353–357. Available from: doi:10.1038/nature08573.

Craig, M.T. & McBain, C.J. (2015) Fast gamma oscillations are generated intrinsically in CA1 without the involvement of fast-spiking basket cells. *The Journal of neuroscience : the official journal of the Society for Neuroscience*. [Online] 35 (8), 3616–3624. Available from: doi:10.1523/JNEUROSCI.4166-14.2015.

Csicsvari, J., Jamieson, B., Wise, K.D. & Buzsáki, G. (2003) Mechanisms of gamma oscillations in the hippocampus of the behaving rat. *Neuron*. [Online] 37 (2), 311–322. Available from: doi:10.1016/S0896-6273(02)01169-8.

El-Gaby, M., Zhang, Y., Wolf, K., Schwiening, C.J., et al. (2016) Archaerhodopsin Selectively and Reversibly Silences Synaptic Transmission through Altered pH. *Cell Reports*. [Online] 16 (8), 2259–2268. Available from: doi:10.1016/J.CELREP.2016.07.057.

Fee, M.S., Mitra, P.P. & Kleinfeld, D. (1996) Automatic sorting of multiple unit neuronal signals in the presence of anisotropic and non-Gaussian variability. *Journal of Neuroscience Methods*. [Online] 69 (2), 175–188. Available from: doi:10.1016/S0165-0270(96)00050-7.

Ferenczi, E.A., Vierock, J., Atsuta-Tsunoda, K., Tsunoda, S.P., et al. (2016a) Optogenetic approaches addressing extracellular modulation of neural excitability. *Scientific Reports*. [Online] 6 (1), 23947. Available from: doi:10.1038/srep23947.

Ferenczi, E.A., Vierock, J., Atsuta-Tsunoda, K., Tsunoda, S.P., et al. (2016b) Optogenetic approaches addressing extracellular modulation of neural excitability. *Scientific Reports*. [Online] 6 (1),

23947. Available from: doi:10.1038/srep23947.

Fisahn, A., Pike, F.G., Buhl, E.. H. & Paulsen, O. (1998) Cholinergic induction of network oscillations at 40 Hz in the hippocampus in vitro. *Nature*. [Online] 394 (6689), 186–189. Available from: doi:10.1038/28179.

Fries, P. (2005) A mechanism for cognitive dynamics: neuronal communication through neuronal coherence. *Trends in Cognitive Sciences*. [Online] 9 (10), 474–480. Available from: doi:10.1016/J.TICS.2005.08.011.

Fries, P. (2015) Rhythms for Cognition: Communication through Coherence. *Neuron*. [Online] 88 (1), 220–235. Available from: doi:10.1016/j.neuron.2015.09.034.

Fries, P., Reynolds, J.H., Rorie, A.E. & Desimone, R. (2001) Modulation of oscillatory neuronal synchronization by selective visual attention. *Science (New York, N.Y.)*. [Online] 291 (5508), 1560–1563. Available from: doi:10.1126/science.291.5508.1560.

Fuchs, E.C., Zivkovic, A.R., Cunningham, M.O., Middleton, S., et al. (2007) Recruitment of Parvalbumin-Positive Interneurons Determines Hippocampal Function and Associated Behavior. *Neuron*. [Online] 53 (4), 591–604. Available from: doi:10.1016/J.NEURON.2007.01.031.

Gloveli, T., Dugladze, T., Saha, S., Monyer, H., et al. (2005) Differential involvement of oriens/pyramidale interneurones in hippocampal network oscillations In vitro. *The Journal of Physiology*. [Online] 562 (1), 131–147. Available from: doi:10.1113/jphysiol.2004.073007.

Gulyás, A.I., Szabó, G.G., Ulbert, I., Holderith, N., et al. (2010) Parvalbumin-containing fast-spiking basket cells generate the field potential oscillations induced by cholinergic receptor activation in the hippocampus. *The Journal of neuroscience : the official journal of the Society for Neuroscience*. [Online] 30 (45), 15134–15145. Available from: doi:10.1523/JNEUROSCI.4104-

10.2010.

Hajos, N. (2004) Spike Timing of Distinct Types of GABAergic Interneuron during Hippocampal Gamma Oscillations In Vitro. *Journal of Neuroscience*. [Online] 24 (41), 9127–9137. Available from: doi:10.1523/JNEUROSCI.2113-04.2004.

Hájos, N. & Paulsen, O. (2009) Network mechanisms of gamma oscillations in the CA3 region of the hippocampus. *Neural Networks*. [Online] 22 (8), 1113–1119. Available from: doi:10.1016/j.neunet.2009.07.024.

Hakim, R., Shamardani, K. & Adesnik, H. (2018) A neural circuit for gamma-band coherence across the retinotopic map in mouse visual cortex. *eLife*. [Online] 7, e28569. Available from: doi:10.7554/eLife.28569.

Hasenstaub, A., Shu, Y., Haider, B., Kraushaar, U., et al. (2005) Inhibitory Postsynaptic Potentials Carry Synchronized Frequency Information in Active Cortical Networks. *Neuron*. [Online] 47 (3), 423–435. Available from: doi:10.1016/J.NEURON.2005.06.016.

Herman, A.M., Huang, L., Murphey, D.K., Garcia, I., et al. (2014) Cell type-specific and time-dependent light exposure contribute to silencing in neurons expressing Channelrhodopsin-2. *eLife*. [Online] 3, e01481. Available from: doi:10.7554/eLife.01481.

Herrmann, C.S. & Demiralp, T. (2005) Human EEG gamma oscillations in neuropsychiatric disorders. *Clinical Neurophysiology*. [Online] 116 (12), 2719–2733. Available from: doi:10.1016/J.CLINPH.2005.07.007.

Hofer, S.B., Ko, H., Pichler, B., Vogelstein, J., et al. (2011) Differential connectivity and response dynamics of excitatory and inhibitory neurons in visual cortex. *Nature Neuroscience*. [Online] 14 (8), 1045–1052. Available from: doi:10.1038/nn.2876.

Hu, H., Gan, J. & Jonas, P. (2014) Interneurons. Fast-spiking, parvalbumin+ GABAergic

568 interneurons: from cellular design to microcircuit function. *Science (New York, N.Y.)*. [Online]
569 345 (6196), 1255263. Available from: doi:10.1126/science.1255263.

570 Kim, D., Jeong, H., Lee, J., Ghim, J.-W., et al. (2016) Distinct Roles of Parvalbumin- and
571 Somatostatin-Expressing Interneurons in Working Memory. *Neuron*. [Online] 92 (4), 902–915.
572 Available from: doi:10.1016/J.NEURON.2016.09.023.

573 Kohus, Z., Káli, S., Rovira-Esteban, L., Schlingloff, D., et al. (2016) Properties and dynamics of
574 inhibitory synaptic communication within the CA3 microcircuits of pyramidal cells and
575 interneurons expressing parvalbumin or cholecystokinin. *The Journal of Physiology*. [Online]
576 594 (13), 3745–3774. Available from: doi:10.1113/JP272231.

577 Lasztóczi, B. & Klausberger, T. (2016) Hippocampal Place Cells Couple to Three Different Gamma
578 Oscillations during Place Field Traversal. *Neuron*. [Online] 91 (1), 34–40. Available from:
579 doi:10.1016/J.NEURON.2016.05.036.

580 Leão, R.N., Mikulovic, S., Leão, K.E., Munguba, H., et al. (2012) OLM interneurons differentially
581 modulate CA3 and entorhinal inputs to hippocampal CA1 neurons. *Nature Neuroscience*.
582 [Online] 15 (11), 1524–1530. Available from: doi:10.1038/nn.3235.

583 Lovett-Barron, M., Kaifosh, P., Kheirbek, M.A., Danielson, N., et al. (2014) Dendritic inhibition in
584 the hippocampus supports fear learning. *Science (New York, N.Y.)*. [Online] 343 (6173), 857–
585 863. Available from: doi:10.1126/science.1247485.

586 Lovett-Barron, M., Turi, G.F., Kaifosh, P., Lee, P.H., et al. (2012) Regulation of neuronal input
587 transformations by tunable dendritic inhibition. *Nature Neuroscience*. [Online] 15 (3), 423–
588 430. Available from: doi:10.1038/nn.3024.

589 Ma, Y., Hu, H., Berrebi, A.S., Mathers, P.H., et al. (2006) Distinct subtypes of somatostatin-
590 containing neocortical interneurons revealed in transgenic mice. *The Journal of neuroscience :*

the official journal of the Society for Neuroscience. [Online] 26 (19), 5069–5082. Available from: doi:10.1523/JNEUROSCI.0661-06.2006.

Mann, E.O., Radcliffe, C.A. & Paulsen, O. (2005) Hippocampal gamma-frequency oscillations: from interneurones to pyramidal cells, and back. *The Journal of Physiology*. [Online] 562 (1), 55–63. Available from: doi:10.1113/jphysiol.2004.078758.

Mann, E.O., Suckling, J.M., Hajos, N., Greenfield, S.A., et al. (2005) Perisomatic Feedback Inhibition Underlies Cholinergically Induced Fast Network Oscillations in the Rat Hippocampus In Vitro. *Neuron*. [Online] 45 (1), 105–117. Available from: doi:10.1016/j.neuron.2004.12.016.

Muller, C. & Remy, S. (2014) Dendritic inhibition mediated by O-LM and bistratified interneurons in the hippocampus. *Frontiers in Synaptic Neuroscience*. [Online] 6, 23. Available from: doi:10.3389/fnsyn.2014.00023.

Nagel, G., Szellas, T., Huhn, W., Kateriya, S., et al. (2003) Channelrhodopsin-2, a directly light-gated cation-selective membrane channel. *Proceedings of the National Academy of Sciences of the United States of America*. [Online] 100 (24), 13940–13945. Available from: doi:10.1073/pnas.1936192100.

Oren, I., Hájos, N. & Paulsen, O. (2010) Identification of the current generator underlying cholinergically induced gamma frequency field potential oscillations in the hippocampal CA3 region. *The Journal of Physiology*. [Online] 588 (5), 785–797. Available from: doi:10.1113/jphysiol.2009.180851.

Oren, I., Mann, E.O., Paulsen, O. & Hájos, N. (2006) Synaptic currents in anatomically identified CA3 neurons during hippocampal gamma oscillations in vitro. *The Journal of neuroscience : the official journal of the Society for Neuroscience*. [Online] 26 (39), 9923–9934. Available from: doi:10.1523/JNEUROSCI.1580-06.2006.

614 Packer, A.M. & Yuste, R. (2011) Dense, unspecific connectivity of neocortical parvalbumin-positive
615 interneurons: a canonical microcircuit for inhibition? *The Journal of neuroscience : the official*
616 *journal of the Society for Neuroscience*. [Online] 31 (37), 13260–13271. Available from:
617 doi:10.1523/JNEUROSCI.3131-11.2011.

618 Penttonen, M., Kamondi, A., Acsady, L. & Buzsaki, G. (1998a) Gamma frequency oscillation in the
619 hippocampus of the rat: intracellular analysis in vivo. *European Journal of Neuroscience*.
620 [Online] 10 (2), 718–728. Available from: doi:10.1046/j.1460-9568.1998.00096.x.

621 Penttonen, M., Kamondi, A., Acsady, L. & Buzsaki, G. (1998b) Gamma frequency oscillation in the
622 hippocampus of the rat: intracellular analysis in vivo. *European Journal of Neuroscience*.
623 [Online] 10 (2), 718–728. Available from: doi:10.1046/j.1460-9568.1998.00096.x.

624 Pfeffer, C.K., Xue, M., He, M., Huang, Z.J., et al. (2013) Inhibition of inhibition in visual cortex: the
625 logic of connections between molecularly distinct interneurons. *Nature Neuroscience*.
626 [Online] 16 (8), 1068–1076. Available from: doi:10.1038/nn.3446.

627 Pike, F.G., Goddard, R.S., Suckling, J.M., Ganter, P., et al. (2000) Distinct frequency preferences of
628 different types of rat hippocampal neurones in response to oscillatory input currents. *The*
629 *Journal of Physiology*. [Online] 529 (1), 205–213. Available from: doi:10.1111/j.1469-
630 7793.2000.00205.x.

631 Pouille, F. & Scanziani, M. (2001) Enforcement of temporal fidelity in pyramidal cells by somatic
632 feed-forward inhibition. *Science (New York, N.Y.)*. [Online] 293 (5532), 1159–1163. Available
633 from: doi:10.1126/science.1060342.

634 Quian Quiroga, R. (2009) What is the real shape of extracellular spikes? *Journal of Neuroscience*
635 *Methods*. [Online] 177 (1), 194–198. Available from: doi:10.1016/J.JNEUMETH.2008.09.033.

636 Quiroga, R.Q., Nadasdy, Z. & Ben-Shaul, Y. (2004) Unsupervised Spike Detection and Sorting with

637 Wavelets and Superparamagnetic Clustering. *Neural Computation*. [Online] 16 (8), 1661–
638 1687. Available from: doi:10.1162/089976604774201631.

639 Ray, S. & Maunsell, J.H.R. (2015) Do gamma oscillations play a role in cerebral cortex? *Trends in*
640 *Cognitive Sciences*. [Online] 19 (2), 78–85. Available from: doi:10.1016/J.TICS.2014.12.002.

641 Royer, S. eacute bastien, Zemelman, B. V, Losonczy, A., Kim, J., et al. (2012) Control of timing, rate
642 and bursts of hippocampal place cells by dendritic and somatic inhibition. *Nature*
643 *Neuroscience*. [Online] 15 (5), 1–10. Available from: doi:10.1038/nn.3077.

644 Savanthrapadian, S., Meyer, T., Elgueta, C., Booker, S.A., et al. (2014) Synaptic Properties of SOM-
645 and CCK-Expressing Cells in Dentate Gyrus Interneuron Networks. *Journal of Neuroscience*.
646 [Online] 34 (24), 8197–8209. Available from: doi:10.1523/JNEUROSCI.5433-13.2014.

647 Schomburg, E.W., Fernández-Ruiz, A., Mizuseki, K., Berényi, A., et al. (2014) Theta phase
648 segregation of input-specific gamma patterns in entorhinal-hippocampal networks. *Neuron*.
649 [Online] 84 (2), 470–485. Available from: doi:10.1016/j.neuron.2014.08.051.

650 Sohal, V.S. (2016) How Close Are We to Understanding What (if Anything) Oscillations Do in
651 Cortical Circuits? *Journal of Neuroscience*. [Online] 36 (41), 10489–10495. Available from:
652 doi:10.1523/JNEUROSCI.0990-16.2016.

653 Sohal, V.S., Zhang, F., Yizhar, O. & Deisseroth, K. (2009) Parvalbumin neurons and gamma rhythms
654 enhance cortical circuit performance. *Nature*. [Online] 459 (7247), 698–702. Available from:
655 doi:10.1038/nature07991.

656 Somogyi, P. & Klausberger, T. (2005) Defined types of cortical interneurone structure space and
657 spike timing in the hippocampus. *The Journal of physiology*. [Online] 562 (Pt 1), 9–26.
658 Available from: doi:10.1113/jphysiol.2004.078915.

659 Spellman, T., Rigotti, M., Ahmari, S.E., Fusi, S., et al. (2015) Hippocampal–prefrontal input supports

spatial encoding in working memory. *Nature*. [Online] 522 (7556), 309–314. Available from: doi:10.1038/nature14445.

Sullivan, D., Csicsvari, J., Mizuseki, K., Montgomery, S., et al. (2011) Relationships between hippocampal sharp waves, ripples, and fast gamma oscillation: influence of dentate and entorhinal cortical activity. *The Journal of neuroscience : the official journal of the Society for Neuroscience*. [Online] 31 (23), 8605–8616. Available from: doi:10.1523/JNEUROSCI.0294-11.2011.

Taniguchi, H., He, M., Wu, P., Kim, S., et al. (2011) A Resource of Cre Driver Lines for Genetic Targeting of GABAergic Neurons in Cerebral Cortex. *Neuron*. [Online] 71 (6), 995–1013. Available from: doi:10.1016/J.NEURON.2011.07.026.

Tukker, J.J., Fuentealba, P., Hartwich, K., Somogyi, P., et al. (2007) *Cell Type-Specific Tuning of Hippocampal InterneuronFiring during Gamma Oscillations*. [Online] 27 (31), 1–6. Available from: doi:10.1523/JNEUROSCI.1685-07.2007.

Tukker, J.J., Lasztóczi, B., Katona, L., Roberts, J.D.B., et al. (2013) Distinct dendritic arborization and in vivo firing patterns of parvalbumin-expressing basket cells in the hippocampal area CA3. *The Journal of neuroscience : the official journal of the Society for Neuroscience*. [Online] 33 (16), 6809–6825. Available from: doi:10.1523/JNEUROSCI.5052-12.2013.

Uhlhaas, P.J. & Singer, W. (2010) Abnormal neural oscillations and synchrony in schizophrenia. *Nature Reviews Neuroscience*. [Online] 11 (2), 100–113. Available from: doi:10.1038/nrn2774.

Uhlhaas, P.J. & Singer, W. (2006) Neural Synchrony in Brain Disorders: Relevance for Cognitive Dysfunctions and Pathophysiology. *Neuron*. [Online] 52 (1), 155–168. Available from: doi:10.1016/j.neuron.2006.09.020.

Urban-Ciecko, J. & Barth, A.L. (2016) Somatostatin-expressing neurons in cortical networks. *Nature*

683 *Reviews Neuroscience*. [Online] 17 (7), 401–409. Available from: doi:10.1038/nrn.2016.53.

684 Veit, J., Hakim, R., Jadi, M.P., Sejnowski, T.J., et al. (2017) Cortical gamma band synchronization
685 through somatostatin interneurons. *Nature Neuroscience*. [Online] 20 (7), 951–959. Available
686 from: doi:10.1038/nn.4562.

687 Whittington, M.A., Traub, R.D. & Jefferys, J.G.R. (1995) Synchronized oscillations in interneuron
688 networks driven by metabotropic glutamate receptor activation. *Nature*. [Online] 373 (6515),
689 612–615. Available from: doi:10.1038/373612a0.

690 Wierenga, C.. & Wadman, W.. (2003) Functional relation between interneuron input and
691 population activity in the rat hippocampal cornu ammonis 1 area. *Neuroscience*. [Online] 118
692 (4), 1129–1139. Available from: doi:10.1016/S0306-4522(03)00060-5.

693 Womelsdorf, T. & Everling, S. (2015) Long-Range Attention Networks: Circuit Motifs Underlying
694 Endogenously Controlled Stimulus Selection. *Trends in Neurosciences*. [Online] 38 (11), 682–
695 700. Available from: doi:10.1016/J.TINS.2015.08.009.

696 Yamamoto, J., Suh, J., Takeuchi, D. & Tonegawa, S. (2014) Successful Execution of Working
697 Memory Linked to Synchronized High-Frequency Gamma Oscillations. *Cell*. [Online] 157 (4),
698 845–857. Available from: doi:10.1016/J.CELL.2014.04.009.

699 Zar, J.H. (1999) Biostatistical analysis. In: *Prentice Hall*. 4th edition. Englewood Cliffs, New Jersey.
700 p. 929.

701 Materials and Methods

702 Transgenic mice

703 All procedures were performed according to the United Kingdom Animals Scientific Procedures Act
704 (ASPA) 1986 and the University of Oxford guidelines. Adult (older than 8 weeks, both male and

female) PV-cre (B6;129P2-Pvalbtm1(cre)Arbr/J), PV-cre-Ai9 (PV-Cre x Gt ROSA (CAG-tdTomato) Hze/J), and SST-cre mice (Sst tm2.1(cre)Zjh/J) were used for all experiments.

Stereotaxic viral injections

Anaesthesia was induced in mice with 4 % isoflurane/medical oxygen mixture (2 L per min). The area around the head was shaved and cleaned in preparation for scalp incision. Anaesthesia was subsequently maintained using 1.5 - 2.5 % isoflurane at a rate of 2 L per min. Before the onset of the procedure a cocktail of systemic peri-operative analgesics (Metacam 1 mg/Kg and Vetergesic 0.1 mg/Kg) and a local analgesic (Marcaine 10mg/Kg) were administered subcutaneously (Oxford University Veterinary Services). Following, antibiotic solution was applied on the head and an incision of the scalp was performed that allowed a small craniotomy to be made. A 33/34-gauge needle was attached on a Hamilton Microliter Syringe and used to inject the virus solution at a rate of ≈100 nL/min (viral concentration ≈ 10^{12} genome copies per mL). After every injection, the needle was left stationary for at least three minutes to allow diffusion of virus in the surrounding area. The virus solution was injected with the aid of a stereotaxic frame into ventral CA3 area of hippocampus (2.7 mm caudal and 2.75 mm lateral from Bregma). A total of 600 - 800 nL were injected at two depths (300 - 400 nL at 3.1 mm and 300 - 400 nL at 2.7 mm). Following the injection, local analgesic (Marcaine 10 mg/Kg) was applied on the incised scalp before it was sutured. The animals were then transferred in a heating chamber and allowed to recover. The animals were monitored, and welfare scored in the following days to ensure that they properly recovered after surgery. Injected mice were assessed for viral expression after a minimum of 3 weeks. All viral constructs were acquired from Vector Core Facilities, Gene Therapy Centre (North Carolina, UNC). Viral constructs used: AAV5-EF1a-DIO-ChR2-mCherry, AAV5-EF1a-DIO-ChR2-eYFP, AAV-EF1a-DIO-Arch3.0-EYFP, AAV-Ef1a-DIO-hChR2(E123T-T159C)-p2A-mCherry-WPRE (Dr. Karl Deisseroth), and AAV-CAG-FLEX-ArchT-GFP (Dr. Ed Boyden).

***Ex vivo* brain slice preparation**

Mice were anaesthetised using 4 % isoflurane (Oxford University Veterinary Services) and were sacrificed by decapitation after the pedal reflex was abolished. Brains were extracted in warm (30 - 35 ^{o}C) sucrose solution (34.5 mM NaCl, 3 mM KCl, 7.4 mM $MgSO_4$.7H2O, 150 mM sucrose, 1 mM $CaCl_2$, 1.25 mM NaH_2PO_4, 25 mM $NaHCO_3$ and 15 mM glucose) and transverse hippocampal slices

of 350 µm thickness were cut using a Leica vibratome (VT 1200S) (Huang et al. 2013). Slices were then immediately placed in an interface storing chamber containing warm (30 - 35 ^{o}C) aCSF (126 mM NaCl, 3.5 mM KCl, 2 mM $MgSO_4$-$7H_2O$, 1.25 mM NaH_2PO_4, 24 mM $NaHCO_3$, 2 mM $CaCl_2$ and 10 mM glucose) at least one hour to equilibrate. All solutions were bubbled with 95% O_2 and 5% CO_2 beginning 30 minutes before the procedure until the end of the experiment.

Electrophysiology

Extracellular recordings were conducted in an interface recording chamber at 33-34 ^{o}C. Visualisation of the slices and electrode placement was performed using a Wild Heerbrugg dissection microscope. Local field potentials were recorded by inserting a borosilicate glass electrode filled with aCSF (tip resistance = 1 - 5 MΩ) in CA3 pyramidal layer. Data were acquired and amplified (x 10) by Axoclamp 2A (Molecular Devices). The signal was further amplified x 100 and low pass filtered at 1 KHz (LPBF-48DG, NPI Electronic). The signal was then digitised at 5000 samples per second by a data acquisition board (ITC-16, InstruTECH) and recorded from the IgorPro (Wavemetrics). Gamma oscillations were induced by the application of 5 µM carbachol (Cch). The LFP signal was quantified using real-time fast Fourier transform (FFT) analysis and oscillations were detected by a peak in the power spectrum at low -band frequencies (25 Hz - 49 Hz). For unit recordings a linear 16 channel tungsten multi-electrode array (MEA; MicroProbes) was lowered in the CA3 subfield. The array channels had 100 µm spacing to ensure full coverage of the hippocampus. The MEA was mounted on an RHD2132 Amplifier board and connected to the RHD2000 USB Interface Board (Intaan Technologies). Data were acquired at a rate of 20000 samples per second using the RHD2000 rhythm software (Intaan Technologies).

Intracellular recordings were always conducted in a single submerged chamber (26 - 32 ^{o}C) using borosilicate glass pipettes (5-12 M). The signal was acquired through the MultiClamp 700B amplifier (Molecular Devices) and digitised at a rate of 10000 samples per second by a data acquisition board (ITC-18, InstruTECH) and was then recorded using the Igor Pro software. The signals were low pass filtered (Bessel) at 10 kHz for current clamp mode and 3 kHz for voltage clamp (VC) mode. Slice and cell visualisation were achieved using oblique illumination and monitored through a HAMATATSU ORCA - ER digital camera. Filtered white LED (460 +/- 30 nm, 1.53 mW, Thor Labs) via epi-illumination was used to activate channelrhodopsin (ChR2). Filtered white LED (525 +/-20 nm, 1.45 mW, Thor Labs) via epi-illumination was used to activate archaerhodopsin (Arch). For a power of 1.5 mW, the illuminated area is 3.68 mW / mm^2. Cell attached recordings were performed in current

771 clamp (IC) mode (Multiclamp software) using glass pipettes filled with aCSF. For whole cell current
772 clamp recordings pipettes were filled with internal solution containing 110 mM KGluconate, 40 mM
773 HEPES, 2 mM ATP-Mg, 0.3 mM GTP-NaCl, 4 mM NaCl, (3-4 mg/ml biocytin, Sigma). For whole cell
774 voltage recordings pipettes were filled with internal solution containing 140 mM Cesium
775 methanesulfonate, 5mM NaCl, 10 mM HEPES, 0.2 mM EGTA, 2 mM ATP-Mg, 3 mM GTP-Na, 5 mM
776 QX-314, (3-4 mg/ml biocytin). Series resistance compensation was not performed in all cells
777 included for analysis. For perforated patch recordings the tip of the pipette was filled with a KCl-
778 containing solution (150 mM KCl and 10mM HEPES, pH 7.2-7.3; Osmolality 300 mOsmol/Kg). The
779 rest of the pipette was filled with the same KCl solution containing 5 µM gramicidin D (1:1000 DMSO
780 dilution, Sigma) and 10 µM Fluorescein (Sigma) to visualise if there was spontaneous rupture of the
781 membrane during patching experiments.
782
783 **Light delivery**
784 For photo-activation (ChR2) experiments, light illumination was delivered through a fibre optic using
785 a blue LED (470 +/- 20 nm, Thorlabs, M470F3; max power at fibre optic tip = 10 mW). For photo-
786 inhibition (Arch) experiments light illumination was delivered through a fibre optic by a green LED
787 (530 +/- 30 nm, Thorlabs, M530F2; maximum power at fibre optic tip = 4.25 mW) and with an amber
788 LED (595 +/- 20nm, Doric, maximum power at fibre optic tip = 5 mW). LED module output was
789 controlled using the Igor Pro software. Laser photo-inhibition experiments were also performed
790 with a green laser (MatchBox series, 532 +/- 0.5 nm, maximum power at fibre optic that was used
791 approx. 40 mW). In these experiments the data were acquired at a rate of 10000 samples per second
792 using IgorPro. The laser was operated manually, and the light duration was recorded using an
793 Arduino Uno board that created a digital time stamp. Experiments were only included if the laser
794 illumination duration was between 19.6 - 20.7 seconds. The area of light illumination was estimated
795 to have a diameter of 1 - 2 mm and therefore for a power of 10 mW the light intensity was between
796 0.8 - 3.2 mW / mm^2.
797
798
799 **Histology and imaging**
800 After electrophysiological recordings, acute brain slices were fixed in 4 % PFA overnight. Slices were
801 kept in PBS (Phosphate Buffered Saline: 1.37 mM NaCl, 2.7 mM KCl, 10 mM Na_2HPO_4, 2 mM KH_2PO_4)
802 at 4 ^oC for short-term storage. For biocytin labelling the slices were washed with 1X PBS 3-4 times
803 and permeabilized with freshly prepared 0.3 %-Triton 1X PBS for 4 - 5 hours. Streptavidin conjugated

804 to Alexa FluorTM 488 (Invitrogen S32355) in PBS-T 0.3 % (1:500) was incubated overnight at 4 ^{o}C.
805 The slices were then washed 4 - 5 times in PBS for 2 hours. Slices were mounted on glass slides using
806 mounting media (DAKO). Confocal images (1024 x 1024) were acquired on a Zeiss LSM700 upright
807 confocal microscope using the 10x air objective and digitally captured using the default LSM
808 acquisition software. Pyramidal cell reconstruction was performed on neuron studio and simple
809 neurite tracer plugin on Fiji.
810
811 **Analysis of local field potentials**
812 In order to characterise and analyse the oscillations, a hanning window was applied and the power
813 spectra were calculated as the normalised magnitude square of the FFT (Igor Pro). The 50 Hz and
814 100 Hz frequencies were not included in the analysis to exclude the mains noise and its harmonic
815 component. The oscillation amplitude was quantified firstly by measuring the peak of the power
816 spectrum termed as peak power and secondly by measuring the area below the power spectrum
817 plot in the gamma-band range (20 - 100 Hz) termed as power-area. The peak frequency of the
818 oscillation was obtained by measuring the frequency at which the peak of the power spectrum
819 occurred in the gamma-band range. In order to quantify when Cch-induced oscillations where
820 abolished upon light stimulation and to exclude the peak frequencies of those oscillations from
821 further analysis one of the two criteria had to be met. Firstly, an auto-correlation of the oscillations
822 was computed and was fitted with a Gabor function $(f(x) = (A * cos(2\pi * f * x)) * e -$
823 $x2/2 * tau)$. The first criterion was met if the resulting Gabor fit had a linear correlation
824 coefficient, r > 0.7 and product of $\sqrt{f * tau}$ > 0.1 (> 0.15 for frequencies higher than 50 Hz). The
825 second criterion was a power-area bigger than 125 μV^2 in the range of +/- 5 Hz of the peak
826 frequency. The power-area was always included in the analysis even if oscillations were abolished.
827 The power spectrum analysis for *de novo* oscillations was performed in the range of 52 – 149 Hz
828 with the only criterion for oscillation presence being that the power-area in +/- 5 Hz of the peak
829 frequency was larger than 40 μV^2. Hilbert transforms were used to obtain instantaneous gamma
830 magnitude for sinusoidal modulation of gamma oscillations (band-pass filtered 20 - 120 Hz). For
831 visualisation purposes the magnitude of the continuous wavelet transform was used normalised by
832 max value (Morlet wavelet; nondimensional frequency = 6).
833
834 **Spike detection and analysis**
835 Unit detection was performed using custom-written procedures in MATLAB (Mathworks).
836 Extracellular spikes from the 16 channel MEA were detected as described before by Quiroga and

colleagues (Quiroga, Nadasdy & Ben-Shaul, 2004; Quian Quiroga, 2009). Briefly, the MEA data were processed with an elliptical band-pass filter (for spike detection: 4th order, 300 - 3000 Hz, for spike sorting: 2nd order, 300 - 6000 Hz). Spikes were detected as signals exceeding 5 standard deviation (s.d.) of the noise $5 * \sigma n = median\{|x| / 0.6745\}$. Signals that exceeded 10 times the s.d. of the detected spike amplitudes were eliminated as artefacts/population spikes. Subsequently, spikes that had peaks occurring at the same time (< 0.1 ms) across channels were grouped together as one unit. This prevented detection of the same unit more than once. Clustering of the detected spikes was performed using custom-written procedures in Igor Pro. A spike sorting procedure adapted from Fee and colleagues was used to explore whether neurons displaying specific spike waveforms were selectively recruited by optogenetic stimulation (Fee, Mitra & Kleinfeld, 1996). Briefly, spike metrics were converted into z scores, over-clustered using an in-built k-means algorithm, and progressively aggregated if the intercluster distance was <2.5 and merging did not produce more violations of refractory period of 2 ms. Analysis was performed on the clustered spikes, with auto-correlation and cross-correlation plots used to validate the clustering procedure. Spike metrics from the average waveform for each cluster were used to identify different waveform types via a k-means algorithm. This clustering procedure is likely to be conservative, and underestimate the firing rate of individual neurons, but was deemed sufficiently robust to detect any bias in optogenetic recruitment. A single unit cluster was identified if it i) had less than 1.4 % of its total spike waveforms within 2 ms of its refractory period and ii) consisted of more than 800 members. When a cluster did not obey these criteria, it was merged with other clusters that had similar action potential waveforms giving rise to a multi-unit cluster.

Clusters were identified as expressing ChR2 if the spike rate in the first 100 ms of the step stimulus was 3 s.d. above the baseline spike rate. The remaining clusters were classified based on the the delay between the negative and positive peaks in the average waveform as fast-spiking (<0.6 ms) or regular-spiking (>=0.6 ms). The Activation Index was calculated over the last second of the step stimulus as the difference between the light-induced and baseline spikes rates divided by their sum, and designed to measure sustained firing. The Theta Modulation Index was calculated as the rank correlation coefficient between the spike time histogram and the theta-modulated amplitude of the light stimulus.

Statistics

Repeated measures ANOVA (rmANOVA) was performed in SPSS with Greenhouse-Geisser correction where required (i.e. significance in Mauchly's test for sphericity) and followed by

Bonferroni-corrected post-hoc paired t-tests. Linear correlations, circular correlations, and Bonferroni-corrected one sample t-tests were performed using Igor Pro. Scatter-bar charts were generated using PRISM. Circular statistics of spike phase relative to ongoing oscillations in the LFP were calculated using in-built functions in Igor Pro. The measurements spiking rates deviated from normality, and were analysed using non-parametric statistical tests performed in SPSS: differences between cell types were analysed using Kruskal-Wallis Test, followed by posthoc Dunn's test, with Bonferroni correction for multiple comparisons. Differences across stimulus types (step and theta) were analysed using the Wilcoxon signed rank test, and the significance of modulation indices analysed using the one-sample Wilcoxon signed rank test (H_0=0). In all figures, the bar charts display the average value and the error bars represent the standard error of the mean, unless explicitly stated otherwise. Stars represent significance values where * $p < 0.05$, ** $p < 0.01$ and *** $p < 0.001$.